CZECH TECHNICAL UNIVERSITY IN PRAGUE

Faculty of Mechanical Engineering

Department of Process Engineering

Master's Thesis

POWER CONSUMPTION OF IMPELLERS AT NON-STANDARD LIQUID LEVEL IN TANK

Acedemic year 2020-2021

Supervisor
Ing. Jiri Moravec, Ph.D.

Author
Janakiraman Kubendran

MASTER'S THESIS ASSIGNMENT

I. Personal and study details

Student's name: **Kubendran Janakiraman** Personal ID number: **490260**

Faculty / Institute: **Faculty of Mechanical Engineering**

Department / Institute: **Department of Process Engineering**

Study program: **Mechanical Engineering**

Branch of study: **Process Engineering**

II. Master's thesis details

Master's thesis title in English:

Power consumption of impellers at non-standard liquid level in tank

Master's thesis title in Czech:

Příkon míchadel při nestandardní výšce hladiny kapaliny v nádobě

Guidelines:

- Based on a literature study, describe the effect of basic parameters of mixing equipment on power consumption of high-speed impellers. Focus especially on effects of impeller diameter and its distance from vessel bottom and from liquid level.
- Carry out experiments to determine power consumption of a chosen type of impeller (specified by supervisor) in a standard configuration of mixing apparatus. In case of bad COVID-19 situation, the data will be provided by supervisor.
- Create a numerical model having the same parameters as the equipment used in experiments and use it for determining the power consumption of the impeller. Validate the numerical model by comparison of the values obtained from both, CFD and experiments, and adjust the numerical model if necessary.
- Use the validated numerical model for determining power consumption of the impeller at different liquid levels in the tank and discuss the obtained results.

Bibliography / sources:

According to the recommendation of Thesis supervisor.

Name and workplace of master's thesis supervisor:

Ing. Jiří Moravec, Ph.D., Department of Process Engineering, FME

Name and workplace of second master's thesis supervisor or consultant:

Date of master's thesis assignment: **21.04.2021** Deadline for master's thesis submission: **10-09-2021**

Assignment valid until: **19.09.2021**

Ing. Jiří Moravec, Ph.D.	prof. Ing. Tomáš Jirout, Ph.D.	prof. Ing. Michael Valášek, DrSc.
Supervisor's signature	Head of department's signature	Dean's signature

III. Assignment receipt

The student acknowledges that the master's thesis is an individual work. The student must produce his thesis without the assistance of others, with the exception of provided consultations. Within the master's thesis, the author must state the names of consultants and include a list of references.

Date of assignment receipt

Student's signature

I confirm that this diploma work was disposed of by me and independently, under the leadership of my thesis supervisor. I stated all sources of the documents and literature.

Date : _____ Kubendran Janakiraman

_____

`

ACKNOWLEDGEMENTS

I would like to acknowledge my supervisor, Ing. Jiri Moravec Ph.D., for his availability and interest. Thank you for the time and professionalism you have dedicated to me.

I also owe a great debt to the city of Prague, which welcomed me two years ago and offered me wonderful opportunities to study, work, and also great friendships.

Today, the great satisfaction recompenses all the efforts made. Every small step brought me to the end of this journey and the beginning of the next. But I did not do it all alone.

And I want to thank my family. You have been with me all these years and have always been willing to support and encourage me when I needed it most. And you have always succeeded.

I am also thankful to all my friends, fundamental elements in such a different historical moment, characterized by distance. We have always found a way to be together, even if we were far away. And finally, thanks to everyone who believed in me, I hope I have given you some satisfaction.

Thank you

Kubendran Janakiraman

ANNOTATION SHEET

Name: Janakiraman

Surname: Kubendran

Title Czech: Příkon míchadel při nestandardní výšce hladiny kapaliny v nádobě

Title English: Power consumption of impellers at non-standard liquid level in tank

Scope of work: Number of pages : 69

Number of figures : 63

Number of tables : 8

Academic year: 2020/2021

Language: English

Department: Process Engineering

Specialization: Process Engineering

Supervisor: Ing. Jiri Moravec, Ph.D.

Reviewer:

Submitter:

Czech Technical University in Prague. Faculty of Mechanical Engineering, Department of Process Engineering.

Annotation - Czech:

V rešeršní části práce byl popsán vliv základních parametrů míchacího zařízení na příkon rychloběžných míchadel při různých otáčkách míchadel. Hlavním sledovaným parametrem byla výška hladiny kapaliny v nádobě. Byl sestaven numerický model míchané nádoby s axiálním míchadlem s diagonálně zaoblenými lopatkami. Parametry modelu byly voleny stejně jako u reálného zařízení připraveného pro modelové experimentální měření. Pomocí numerických simulací byl stanoven příkon míchadla a jeho příkonové číslo při různých výškách hladiny kapaliny v nádobě a při různých otáčkách míchadla. Numerický model byl validován porovnáním výsledných hodnot s příkonem a příkonovým číslem stanoveným z dat získaných z experimentálních měření.

Annotation - English:

The effects of basic mixing equipment parameters on the power consumption of high-speed impellers at various rotational speeds were defined in a literature study. The impact of the height of the liquid level was the main topic. A numerical model of a mixing vessel with an axial impeller with diagonally rounded blades was created. The model layout was the same as a real layout prepared for experimental measurements. The impeller's power consumption and power number at various liquid levels and rotational speeds were calculated using the numerical simulations. The results were compared to the power consumption and the power number obtained from the experimental measurements to validate the numerical model.

Keywords:

Mixing tank, Impeller, Power consumption, CFD, Power number, Liquid height

Utilization:
For the Department of Process Engineering, Czech Technical University in Prague

TABLE OF CONTENTS

List of Figures

List of Tables

ABSTRACT

Mixing is an essential process in many industries such as chemicals, minerals, food, petroleum, pharmaceuticals, etc. Therefore, the power consumption of the impeller or agitator during mixing will have a greater impact on the operating cost. In this study, the CFD model is developed to study the power consumption of the impeller during the draining and filling of the vessel. The multiple reference frame technique (MRF), the SST K-Omega turbulence model, and the VOF multiphase model are used to study the power demand of the impeller at different liquid heights. Then, the CFD results are compared with the experimental data. In this thesis, the effect of liquid height and impeller speed on impeller power consumption is investigated.

1. Introduction

The term mixing refers to combining materials such as liquid-liquid, gas-liquid, solid-liquid, solid-solid, solid-liquid-gas, etc. Therefore, mixing is an important operation in many industries such as chemicals, food, petroleum, minerals, cosmetics, paper, pharmaceuticals, etc. And some of the operations are mixing and blending specialty chemicals, explosives, fertilizers, dry powdered detergents, glass or ceramics, rubber compounds, gentle mixing during fermentation, mixing of spices, flavors, etc. Additionally, mixing is a critical process because the final quality of the product depends greatly on the quality of mixing. Improper mixing leads to inhomogeneity of the product that lacks consistency with desired attributes such as composition, texture, flavor, reactivity, and particle size.

There are three types of mixing equipment widely used depending on the type of material being mixed, which are blender mixers, heavy duty mixers, and agitator mixer. The blender mixer is mainly used for solid-solid blending, and the heavy-duty mixers are used for highly viscous and pasty materials. Lastly, an agitator mixer equipped with an impeller in the vessel is used to perform mixing of miscible, immiscible liquid or gas.

Mixing is no longer a generic production tool, but a critical and decisive business tool. This is because the profitability of the industry is affected by the power consumption of the impellers. Therefore, the first study performed on power consumption dated to 1934, but the early study based on dimensional analysis developed the dimensionless number such as power number and flow number is created by Rushton and is widely accepted as the definitive work in this area.

The main aim of the thesis is to analyze the effect of the nonstandard liquid level on the power consumption of the impeller. To study this, CFD analysis is used to understand how the power consumption of the impeller is affected by non-standard liquid levels at different rotational speeds of the impeller.

2. Literature review

2.1 Classification of impellers

Generally, the impellers are classified based on the flow types. So, there are three types of impellers mentioned below.

1.Radial-flow impeller

2.Axial flow impeller

3.Tangential flow impeller

2.1.1 Radial flow

Radial impellers are shown in *Figure 1. In* radial flow impellers, the fluid moves perpendicularly to the impeller or the fluid moves sideways during the operation. The displaced fluid will move upwards or downwards and then come back to the center towards the impeller, which only to be pushed to the exterior again to repeat the cycle. Radial impellers were appreciably fit for low-level applications inside long tanks based on the production of higher shear due to the angle of attack.

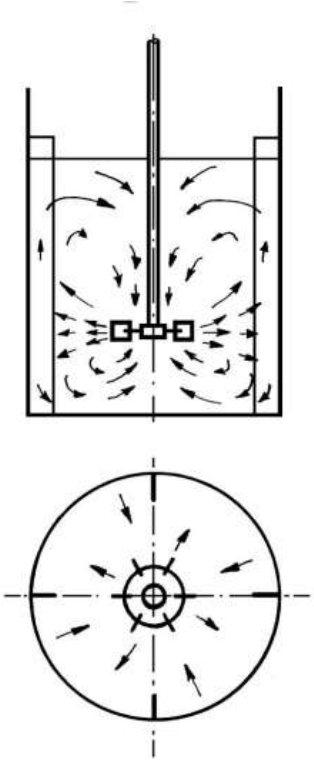

Figure 1 Flow patterns of Radial flow impeller[21]

2.1.1.1 Types of radial-flow impellers

Rushton turbine : Rushton was one of the first impellers studied formally in mixing. Its shape is shown in *Figure 2.* The Rushton turbine consists of a flat disc to maintain constant pressure on either side of the impeller with six vertical blades for radial flow.

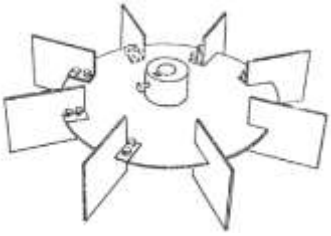

Figure 2 Rushton or flat blade turbine [23]

Curve blade turbine : curved blade turbine, CBT is shown in *Figure 3. This* impeller produces a radial flow pattern with less shear and power consumption than a vertical flat blade turbine. It is used in applications such as heat transfer, high solids content, or low liquid levels.

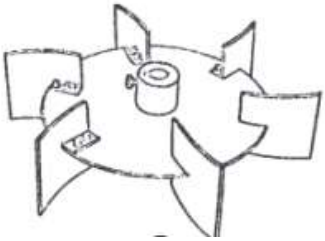

Figure 3 Curve blade turbine [23]

Spiral backswept : Spiral backswept flat bladed turbine is shown in *Figure 4.It is* used as a closed clearance mixing impeller near the bottom of a tank for low viscosity applications. The impeller is used in Smelt Dissolver applications in pulp and paper plants.

Figure 4 Spiral backswept [23]

2.1.2 Axial flow impeller

In fluid motion, axial flow is the movement of the fluid in a cyclic upward and downward pattern. The rotation of the axial flow impeller causes the fluid to move downward and later upward before being pushed down again to repeat the cycle. Axial flow patterns are shown in *Figure 5.*

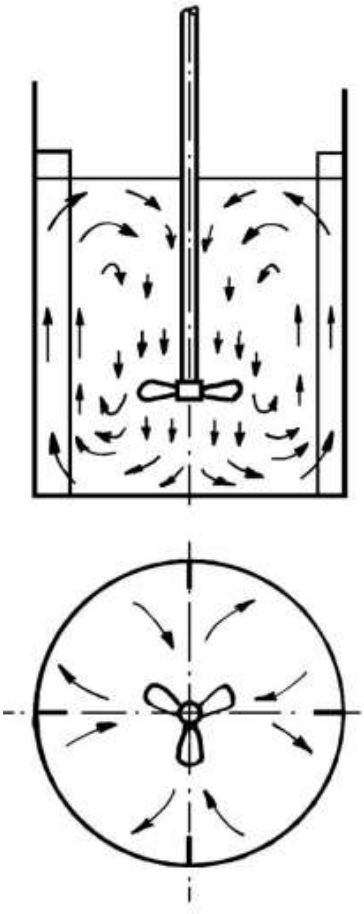

Figure 5 Flow patterns of Axial flow impeller[21]

2.1.2.1 Types of axial flow impeller

The most widely used impellers are

1. Pitched axial impeller: This type of impeller has a blade with different angles. This kind of impeller produces a good balance between shear and fluid motion when rotating. Therefore, it makes them suitable for a wide variety of applications. The example is shown in *Figure 6.*

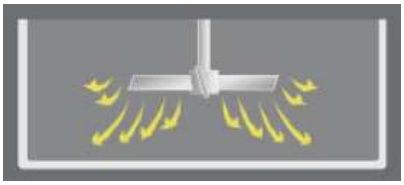

Figure 6 Pitched axial impeller[22]

2.Propeller blade: The propeller impeller is shown in *Figure 7. This* type of impeller is used mostly in mixing for better efficiency. However, they generate less shear compared to the pitch blade impeller.

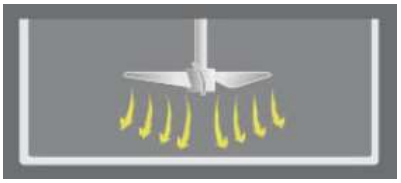

Figure 7 Propeller blade impeller[22]

3. Hydrofoil: The hydrofoil impeller is a group of impellers. An example of such an impeller is shown in *Figure 8.* It is a three-bladed high-efficiency impeller of different types. This axial flow impeller produces the least amount of shear stress in fluids. Their design is great for producing high flow. They can be used for general mixing applications, but they are also an alternative for large-scale mixing applications because they are complicated to manufacture because of their specific shapes.

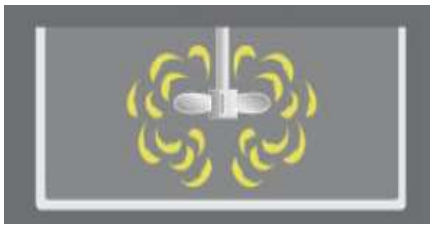

Figure 8 Hydrofoil impeller[22]

2.1.3 Tangential Flow Impeller

The flow pattern of the tangential flow impeller is shown in *Figure 9.* Fluid flow acts in a direction tangent to the circle of rotation around the shaft. If the shaft is placed vertically and centrally, the tangential flow follows a circular path around the shaft and creates a vortex in the liquid.

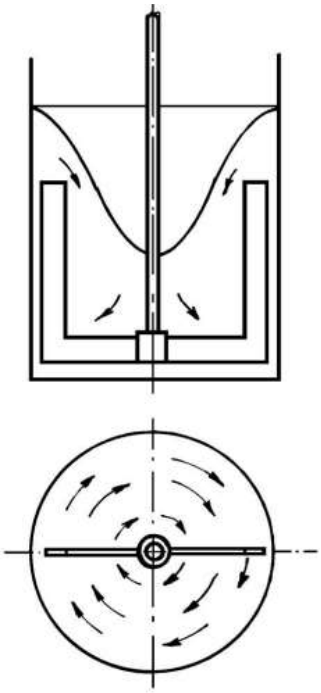

Figure 9 Flow patterns for tangential flow impeller [21]

2.2.Definition of power consumption

Power consumption is defined as the amount of energy or power consumed by the impeller and shaft during operation, or power is the energy per unit of time that has to be transferred from the impeller to the liquid to keep it in motion. Furthermore, power consumption is evaluated by the total force (pressure and shear force) acting on the impeller and blades. Units of power consumption are watts.

$$P = 2\pi NM \qquad (1)$$

where N is the impeller revolution (rps), M is the torque (nm) and P is the power (watt).

2.3.Power number theory

Several investigators have reported[1][2]impeller power characteristics in terms of two dimensionless numbers, the Power number (Np), and the impeller Reynolds number (Re). White and his coworkers (1934) were the first to indicate the chance of correlating impeller power using dimensional analysis and its advantages. A common power relationship as a function of physical and geometric parameters was mentioned [1] [2] as follows:

$$\frac{P}{\rho N^3 D^5} = k\left(\frac{\rho N D^2}{\mu}\right)^a \left(\frac{ND^2}{\mu}\right)^b \left(\frac{T}{D}\right)^c \left(\frac{H}{D}\right)^d \left(\frac{C}{D}\right)^e \left(\frac{P}{D}\right)^f \left(\frac{W}{D}\right)^f \left(\frac{L}{D}\right)^h \qquad (2)$$

The impeller power number is shown by the group on the left-hand side (Np). The impeller Reynolds number (Re) is the first group on the right-hand side of the bracket, while the Froude number (Fr) is the second. The impeller and tank geometry arrangement are taken into consideration in the following terms. The hydrodynamic effect is quantified by the Reynolds number. In swirling systems, the Froude number accounts for the effect of the vortex. Equation (2) is also suggested to be enlarged to incorporate the number and width of the baffles, the spacing between the impellers, and the location of the off-center impellers. All of these extra geometrical parameters can be presented in a format similar to that of Equation (2). Furthermore, the author proposed [3] that the effect of the bottom of the vessel should be considered in the previous analysis because the shape of the bottom of the vessel is a significant geometrical component that affects the recirculation pattern and is also likely to influence the power consumption of the impeller. However, in practical power calculations, the complete version of Equation (2) is rarely employed. If no vortex is present and geometrical similarity is assumed, the equation reduces to

$$Np = k(Re)^a \qquad (3)$$

Furthermore, if the mixing process is carried out in a fully baffled turbulent region at a given configuration geometry, *Equation (3)* reduces to

$$Np = \frac{P}{\rho N^3 D^5} = Constant \qquad (4)$$

Therefore, the dimensionless group of power numbers (Np) represents an important parameter since its knowledge enables the designer to predict the impeller power requirement for a given operation.

2.4. Factors Affecting Power Consumption

2.4.1 Impeller geometry

Power consumption is highly dependent on the design of the impeller like impeller shapes, impeller position, and impeller blade angle.

2.4.1.1 Impeller shape

A CFD study [4] was conducted on the Rushton impeller, shown in *Figure.10(a)* and the modified Rushton impeller with two circular covering plates mounted on the upper and lower sides of the blades (RT-C) is shown in *Figure.10(b*).They found that the power consumption of the modified Rushton impeller (RT-C) is reduced to 18 % compared to the standard Rushton turbine. .

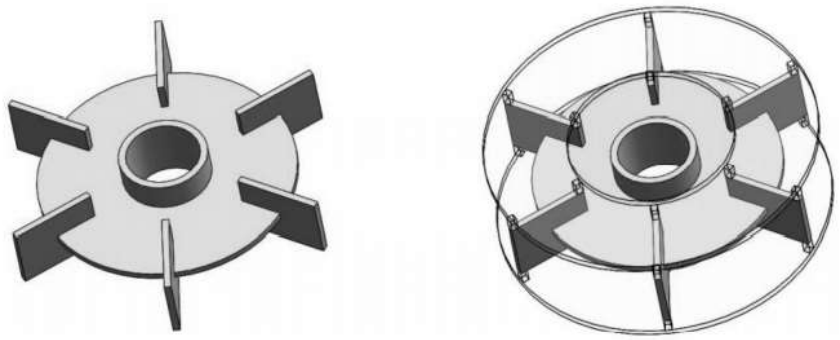

(a) (b)

Figure 10 Rushton impeller (a) standard Rushton impeller (b) modified Rushton impeller(RT-C)

Table 1 Torque and power number of RT and RT-C

Impeller	Torque/N·m	Power number
RT	0.061	4.967
RT-C	0.050	4.072

The torque and power numbers of the standard Rushton impeller(RT) and the modified Rushton impeller (RT-C)are shown in *Table 1.* The simulated power numbers of RT and RT-C were 4.967 and 4.072, respectively. From a quantitative comparison, they found that the power number of RT-C was lower than the power number of RT, about 18% decreased.

The experiment [5] conducted to analyze the effect of the Reynold number and Fourier number on power consumption in the stirred vessel. They concluded that the primary factor affecting power consumption is the size or shape of the impeller. In another study [6], the authors studied the effect of impeller geometry on fluid flow patterns for selected impellers (pitch blade turbine impeller and hydrofoil). The authors observed that the shape with blade twist decreased the power consumption of the impellers.

Early studies [7] carried out on the paddle impeller with a different number of blades showed that the number of blades strongly influences viscous dissipation and power consumption. Figure 11 shows the variation of power consumption with different number of blades(α) which are α = 2,3,4,5,6,7,8. It is clearly shown that the power requirement increases when the number of blades is increased. The 8-blade impeller consumes 2.5 times higher power compared to the 2-blade impeller.

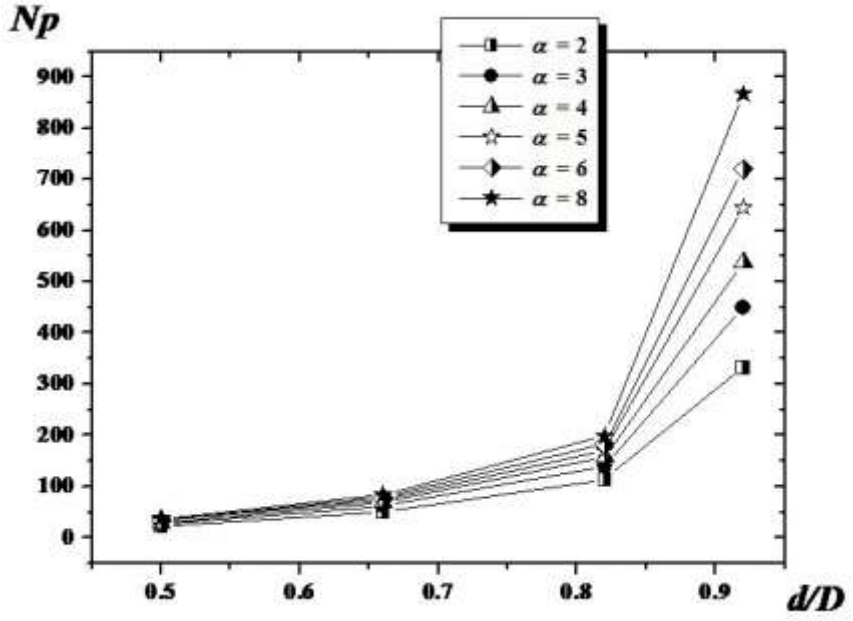

Figure 11 Variation of power consumption with different number of blades [7]

2.4.1.2 Impeller position

Impeller spacing or position plays a vital role in power consumption. The experiment [8] was carried out on a double-bladed impeller with an unbaffled cylindrical flat bottom mixing vessel with an inner diameter of the vessel of 0.185 m. And the working material is chosen as a starch syrup solution with a density of 1300 kg/m^3 and viscosity of about 5 Pa.s. In this experiment, they are using different types of turbine impellers.

In the entire experiment, the same type of impeller with the same size was used as the upper and lower impellers, and both impellers were set symmetrically at half the liquid height level as shown in *Figure 12.* The flow field in the mixing vessel was measured using a particle image velocimeter(PIV).

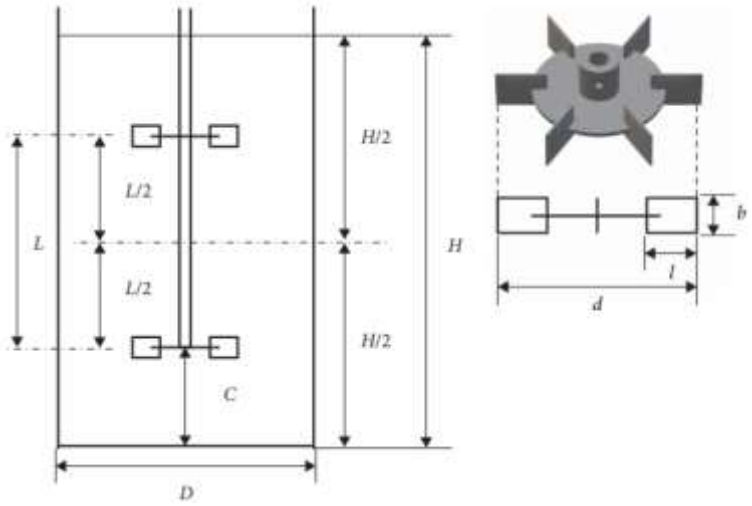

Figure 12 Experimental setup [8]

They revealed that power consumption is strongly dependent on the flow pattern generated by the impeller. The effect of the impeller spacing on the flow pattern and power consumption was studied using turbine impellers in the laminar region. The effect of impeller spacing on the flow pattern was first investigated using particle image velocimetry (PIV). Changes in flow pattern are then mentioned and supported by the ratio of impeller spacing between impellers to impeller blade height(L/b). At L/b =1.0, the double impeller function is kind of a single impeller. The flow between the impellers interacts within the range 1 < L/b < 5. Each of the double impeller functions independently within the 5 L / b range.

$$\frac{(Np.RE)double}{(Np.Re)_{L/b\ =1}} = \left(\frac{L}{b}\right)^{0.20} \qquad (5)$$

Where, $(Np.Re)_{L/b\ =1}$ is $Np.Re$ for double impeller at $\frac{L}{b} = 1$.The power consumption of a double impeller in the range 1 ≤ L/b < 5 can be simply correlated by equation (5), and that of a double impeller in the range 5 < L/b is twice that of a single impeller of the same size power consumption is closely related to the flow pattern and impeller spacing.

2.4.1.3 Impeller blade angle

The experiment [9] was carried out in a horizontal unbaffled vessel with flat side heads of the same dimensions. The inner diameter of the vessel (D) is 240 mm, the length of the vessel (L) is 204 mm, the height of the clear liquid (H) is 204 mm, and the clearance from the bottom of the vessel (C) is 68 mm. The heights of the liquid surface in these two vessels were not equal; the height of the liquid surface in the vertical vessel, Hv, is 186.5 mm, and the diameter of the impeller is 80 mm, the thickness of the blade is 2 mm, the baffle width is 24 mm, and the number of baffle is 4. Tap water was used as a working fluid. And the shaft could rotate at a speed of 100 – 300 rpm. A torque meter unit was used to measure the torque.

A schematic representation of the laboratory equipment is shown in *Figure 13.* and the geometry of the adopted impeller is shown in *Figure 14*. Experiments have been performed using six-blade Rushton disc turbines with various blade pitch angles. The impeller nomenclature is shown in *Figure 15.*

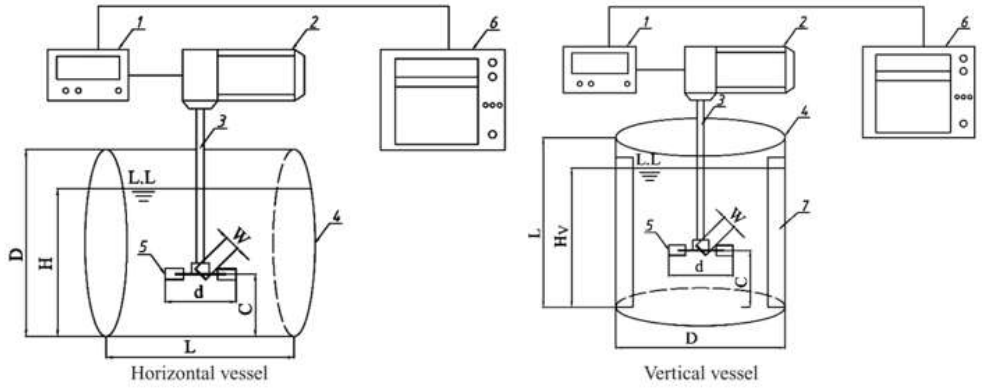

1. Torque gauge, 2.Motor, 3. Shaft, 4.Vessel, 5.Impeller, 6.Graphic recording meter 7. Baffle

Figure 13 Schematic representation of laboratory equipment [9]

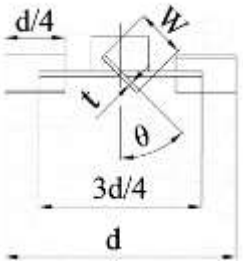

Figure 14 Impeller geometry[9]

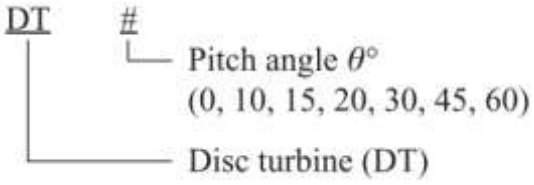

Figure 15 Impeller nomenclature[9]

Finally, they concluded that increasing the impeller pitch blades partially decreases the power number, which means lower power consumption. It can be seen that the power numbers of the impellers with various pitch angles in the vertical and horizontal vessels are shown in *Figure 16.*

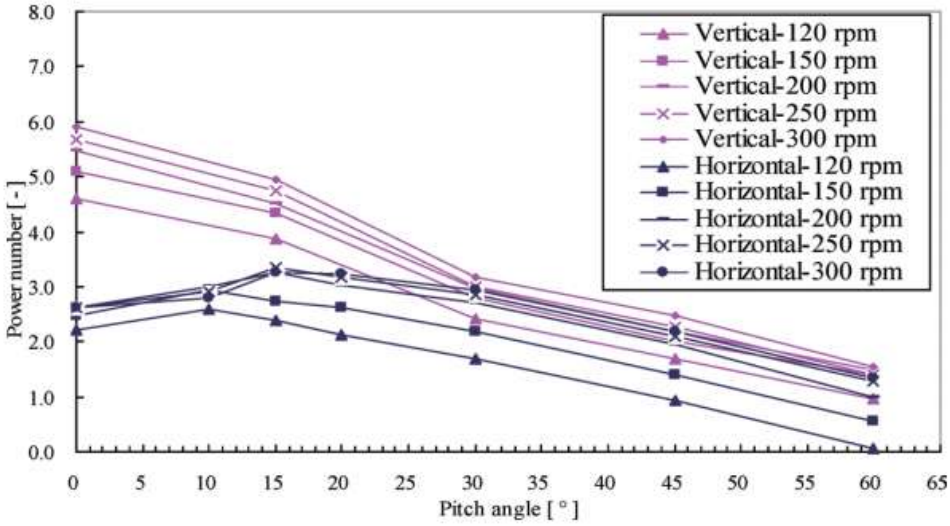

Figure 16 power numbers of the six-blade Rushton disc turbine impeller with various pitch angles in vertical and horizontal vessels [9]

2.4.2 Impeller rotational speed

Impeller rotational speed of the impeller has a significant impact on the power number, while increasing the rotational speed of impeller conveniently increases the power number. The experiment was carried out with a curved blade turbine impeller (CBT), disc turbine (DT), flat blade turbine (FBT), and pitched blade turbine (PBT) with a vessel at three different rotation speeds, which are 300 rpm, 400 rpm, and 500 rpm. The authors concluded that the power number is dependent on the third power of the impeller rotational speed in turbulent region flow according to *equation 4*. Therefore, increasing the rotational speed will increase the power consumption as shown in *Figure 17. The* results obtained here indicate a good agreement with the power relationship of *Equation 3*.

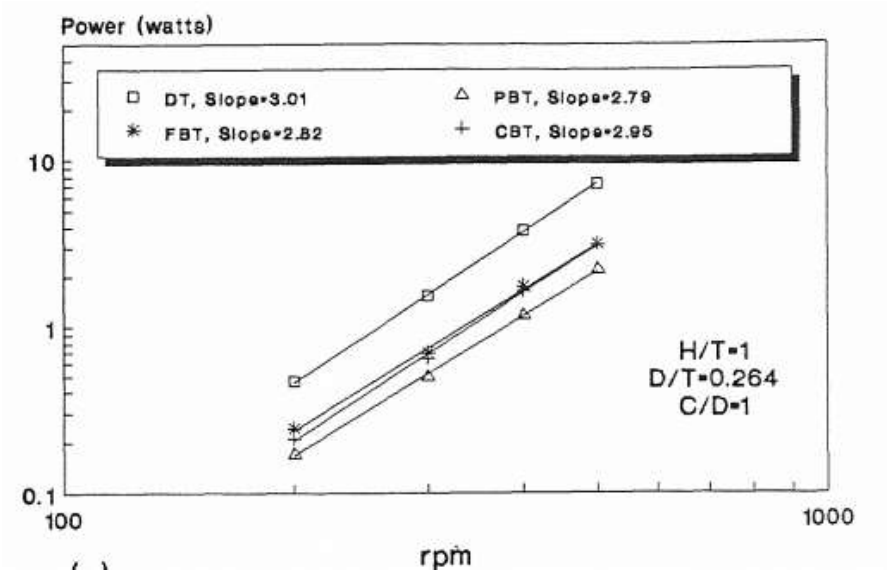

Figure 17 Effect of Agitation Speed on Power[10]

2.4.3 Effect of baffle in power consumption

Power consumption depends not only on the type and number of impellers, the speed of the impeller, and the fluid density, but also on the geometry of the system. To study the power consumption of an impeller in a system with and without baffle. Experimental investigations [12] were carried out in a cylindrical flat bottom vessel of inner diameter = 0.19 m, equipped with four vertical symmetrically located baffles of width b = 0.018 m and in different immersion lengths, L, in the liquid. The vessel was filled with tap water and the liquid height, H, in the vessel was set equal to 1.4 D. Two Rushton turbines of diameter d = 0.52 D were used as dual-impeller stirring devices, with blade length and blade height 0.25 d and 0.20 d, respectively. The clearance of the bottom impeller was equal to 0.5 d.

Figure 18 shows, as an example, the experimental setup for a baffle length L / H = 0.52, that is, p / H = 0.48 where L is the length of the baffle immersed in (m) and p is the distance between the lower edge of the baffles and the bottom of the vessel in (m). Measurements were performed under turbulent flow conditions in the mixing vessel.

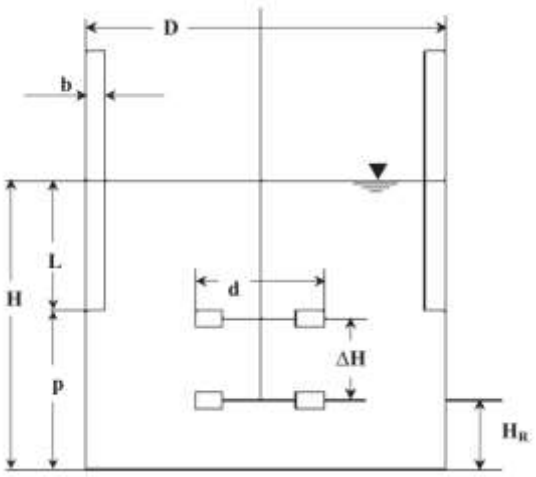

Figure 18 Experimental setup for a baffle length [12]

In *Figure 19, the experimental* results concerning the dependence of the power number (Np) on Re are given comparatively for the fully baffled (p/H = 0) and without baffled (p/H = 1) configurations.

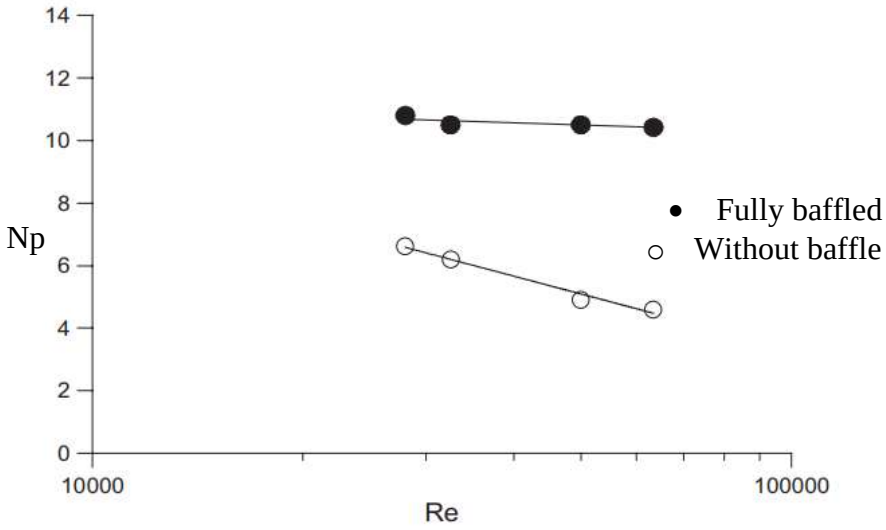

Figure 19 Dependence of the power number (Np) on Re [12]

It clearly shows in *Figure 19.* that the fully baffled vessel consumes more power compared to the vessel without baffle.

2.4.4 Effect of liquid height

The experiment [13] was carried out in a vessel with different axial and radial impellers. They used two types of radial impellers, Rushton turbine (RT) and straight blade (SB), and two types of axial impeller, Rushton turbine 45 ° angle (RT 45) and slit blade (PBT), and used water as a working fluid. They concluded that the power consumption increases when the height of the liquid is decreased.

Another study [15] was carried out in a flat bottom container with a diameter of 400 mm, and the agitator was engaged at 1/3 of the tank height. The tank was filled with water at 20 degrees Celsius. Six inclined blades (PBT) pitched blade turbines were used for the tests. The angles of inclination of the blades with respect to the horizontal plane were as follows: 15°, 30°, 45°, 60° and 75 °. A turbine blade agitator was also tested, for which the angle of inclination of the blade in relation to the horizontal was 90 °. The diameter of the entire impeller was d=133 mm and the width of the blade b =0.2d, and the water is filled with the initial height H=D and the entire test was carried out in turbulent flow with different rotational speeds of the impeller 90,150,210 and 270 RPM. Furthermore, they used a pump to empty the tank with a constant volumetric flow rate about 0.464 dm^3/ min and stopped pumping when the liquid level reaches 5 mm above the impeller and the torque was measured and then the power number (Np) was calculated from equation 6.

$$Np = \frac{P}{N^3 D^5 \rho} = \frac{2\pi NM}{N^3 D^5 \rho} = \frac{2\pi M}{N^2 D^5 \rho} \qquad (6)$$

Early results suggested that for 6PBT with different inclined blade angles, the power consumption was increased during the emptying of vessel. This was due to the hypothesis that the increase in power consumption was due to the change in the axial circulation of the impeller to a more energy-intensive radial circulation. This change was most likely due to the lack of a sufficiently high layer of liquid above the impeller to close the vertical circulation lines of circulation in tanks. Changes in liquid circulation during the setting of the stirrer are shown in *Figure 20.* To test this hypothesis, preliminary tests were carried out on a six-blade stirrer with a blade angle of 90 °, also called a paddle impeller. It is a typical representative of mixers with radial action, for this type of impeller no increase in mixing power was observed as shown in *Figure 21.*

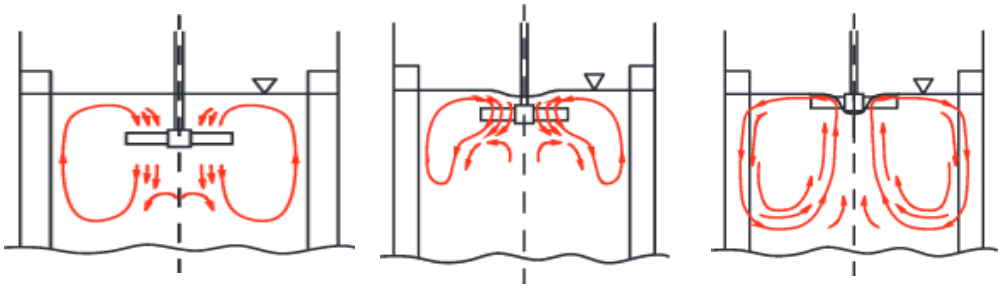

Figure 20 Change in fluid circulation during the ascent of the impeller [15]

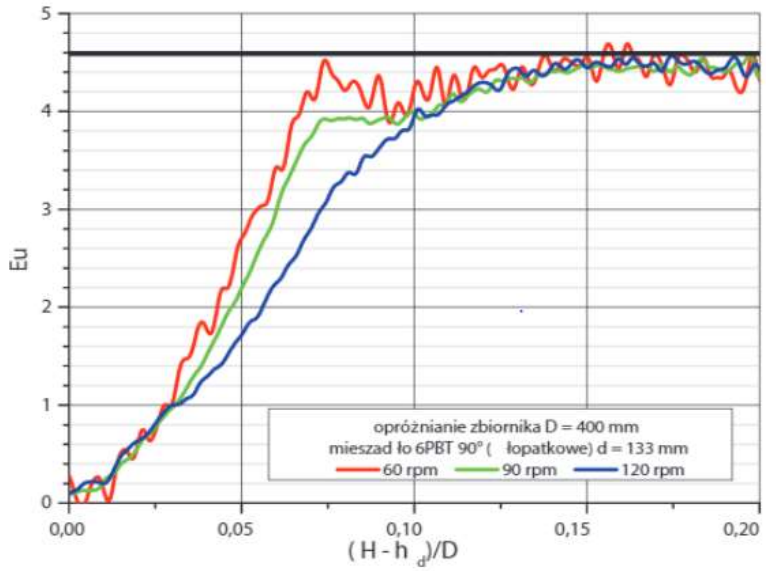

Figure 21 Mixing power changes during emptying the tank with the paddle impeller [15]

The fraction in the horizontal axis H - h_d / D represents the dimensionless liquid level above the impeller from the lowest edge,where H is the instantaneous height of the liquid, and h_d is the distance of the lower edge of the agitator blade from the bottom of the tank.

Furthermore ,they also found that the increase in power demand depended to the greatest extent on the rotational speed of the impeller and to a slightly lesser extent on the angle of inclination of the blade. So, they described the increase in mixing power for turbine blade mixers with inclined blades in the system by this *equation (7).*

$$\frac{Np}{Np_{ref}} = \frac{f(H - h_d)}{D} \qquad (7)$$

In this case, Np skips the instantaneous mixing power number when emptying the tank and duplicates the reference power number for a fully drained tank. Finally, they conclude that the angle of the impeller blade with 15 ° and 90 RPM has more power consumption compared to the other angles and impeller speed shown in *Figure.22*

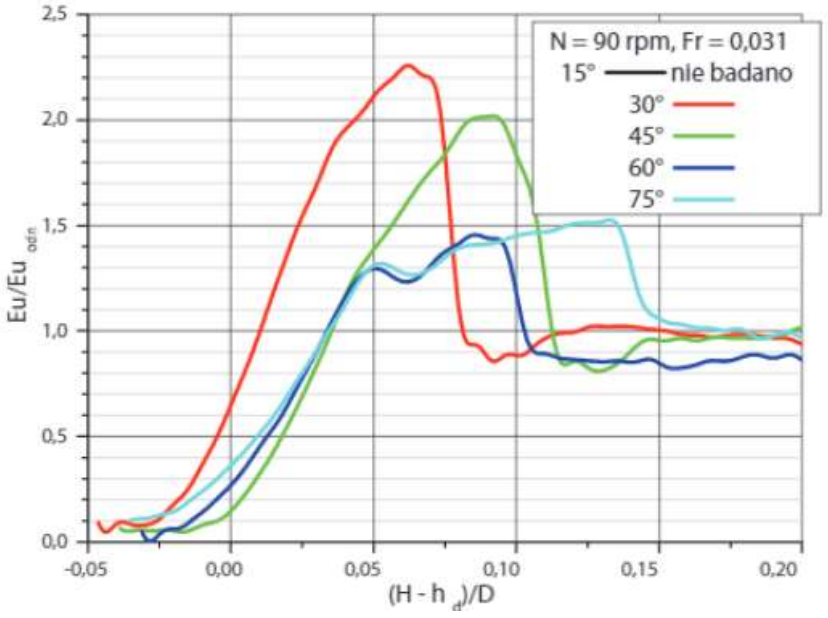

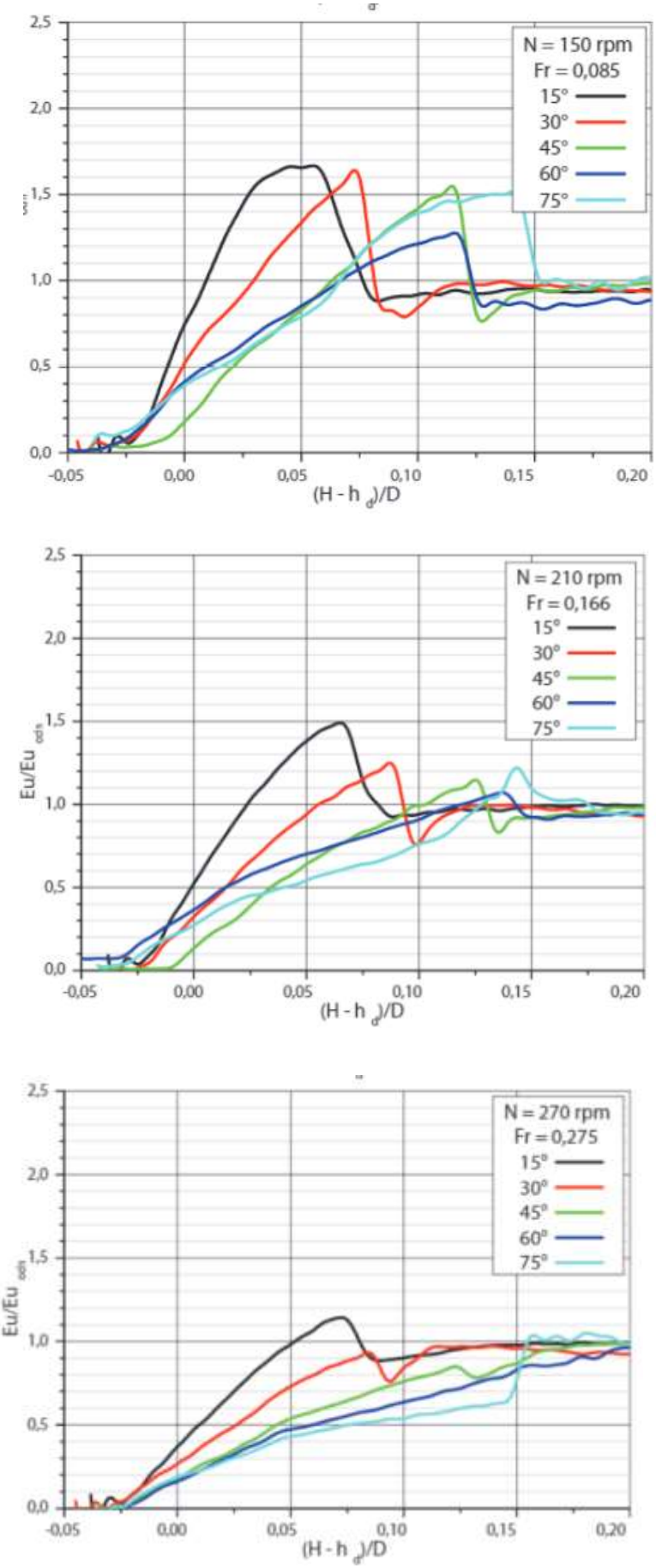

Figure 22 Relative mixing power during emptying the tank for different rotation speeds and blade pitches [15]

On the other hand, they observed changes in the power consumption during draining, when the liquid is pumped upward and downward through the impeller for different rotational speeds. The analysis of this *Figure.23* leads to the conclusion that the largest increase in power consumption occurred when the liquid is drained from the bottom of the mixing tank. The increase in power consumption doubled, even for a small rotational speed(N) and for a small power number (Np) .

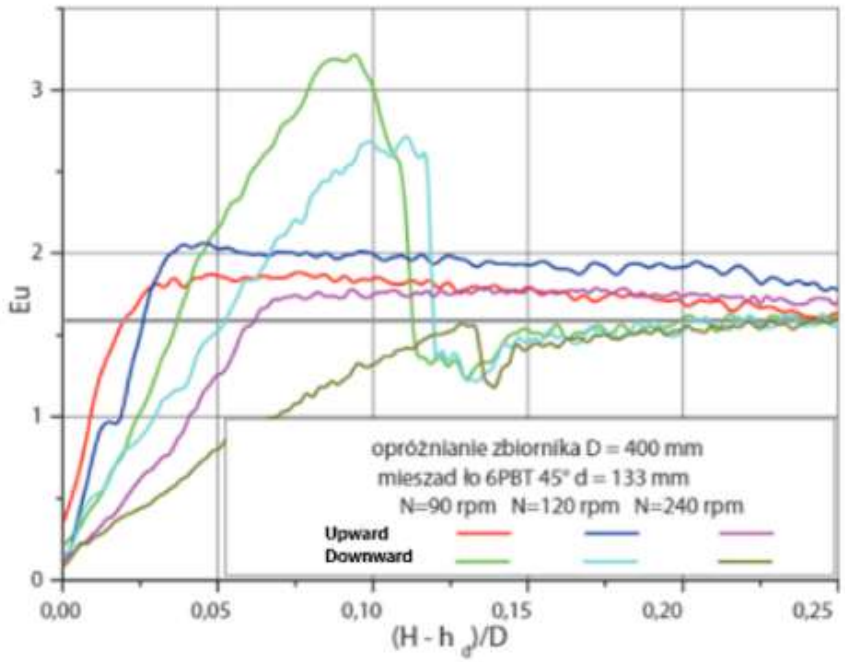

Figure 23 Comparison of mixing power changes during emptying tank [15]

Another experiment conducted [16] in a vessel with flat bottom tanks with diameters (D) of 300 mm and 400 mm equipped with 4 standard baffles (B=0.1D). The tanks were filled with water to height Hp=190 mm and 235 mm, respectively (Hp / D =0.6). For the tests, an impeller with diagonally folded blades (RLL) was used. It was an axial action agitator used to mix the suspensions. The top surface of the agitator blades was always at a height h= 150 mm for the diameter of the impeller d =133 mm and 110 mm for d= 100 mm above the bottom of the tank. They found that the power consumption of the impeller is slightly higher when emptying the tank compared to filling the tank, which is shown in *Figure 24* because when the liquid height above the impeller was reduced to 10 mm during emptying the tank, a quite rapid change in circulation occurred because the impeller forces the liquid to the bottom of the mixer. Thus, change in fluid flow circulation from axial circulation to radial circulation. During filling the tank, the height of the liquid is constantly increasing, and when the liquid height goes above 10 mm, the impeller pumps the liquid up, so the flow circulation is changed from radial to less power-consuming axial circulation.

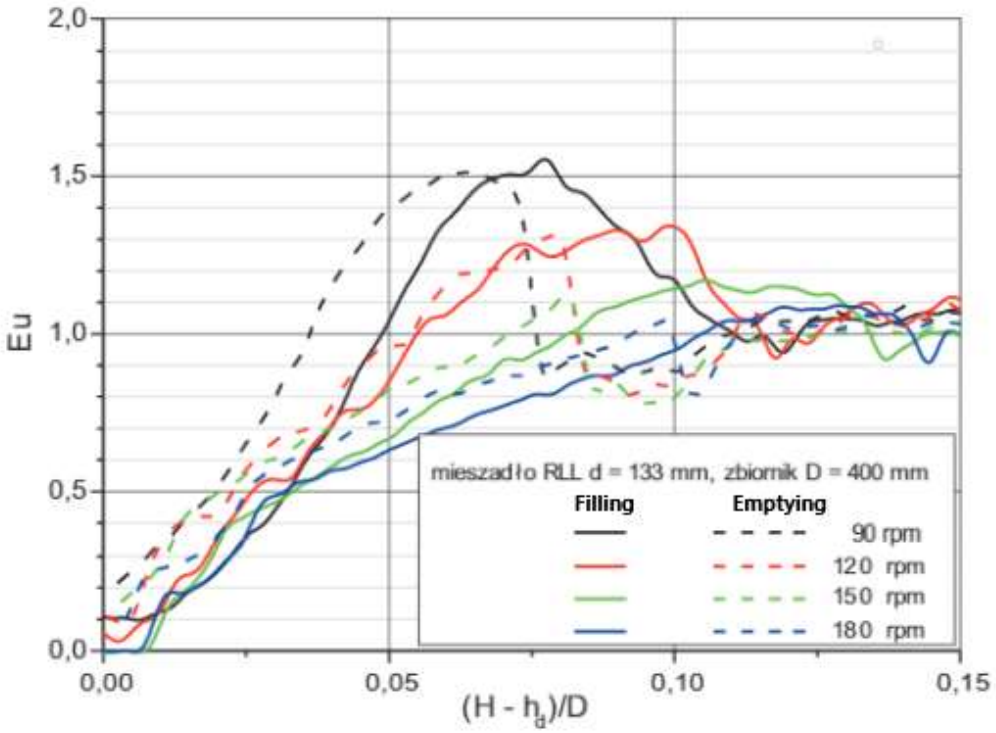

Figure 24 Comparison of mixing power changes During emptying and filling tank [16]

2.4.5 Effect of bottom clearance

The experiment [10] was carried out on four impellers which are disc turbine (DT), 45 ° pitched blade turbine (PBT), flat blade turbine (FBT), and curved blade turbine (CBT) to analyze the effect of the bottom clearance on the power consumption of the impeller. The authors observed that, for the case of a disc turbine, the power number increases when the bottom clearance increases, as shown in *Figure 25 &Table.2*. At low level , the bottom circulation of the disc turbines is reduced, producing a lower power consumption.

The 45 ° pitch blade turbine (PBT) exhibits radial and axial flow patterns. The effect of clearance on the power number was different due to the mixed flow pattern. Contrary to the behavior of the disc turbine, when the clearance is increased, the power number decreases, as shown in *Figure.25 &Table.2.* At low clearance, the impeller stream hits the bottom of the vessel with higher velocity, causing a sharp change in the flow direction, which dissipates more energy. As a result, an increase in power was obtained. For the flat blade turbine (FBT), the power number decreases as the clearance increases. Finally ,for the case of the curved blade turbine (CBT) or the backswept turbine, the power number decreased when the clearance increased [10]. The results are plotted in *Figure 25* and tabulated in *Table 2*.

Table 2 Effect of Clearance on Power Number

Ratio of off-bottom clearance to impeller diameter(C/D)	power number, Np			
	DT	PBT	FBT	CBT
1/6	3.34	1.90	2.57	2.26
1/2	4.35	1.64	2.16	2.13
1	4.90	1.49	2.39	2.06
3/2	4.96	1.39	2.39	1.99
2	5.10	1.34	2.14	2.05

As we can see in Figure 25 and Table 2, the pitched blade turbine consumes the least power consumption due to the mixed flow pattern created.

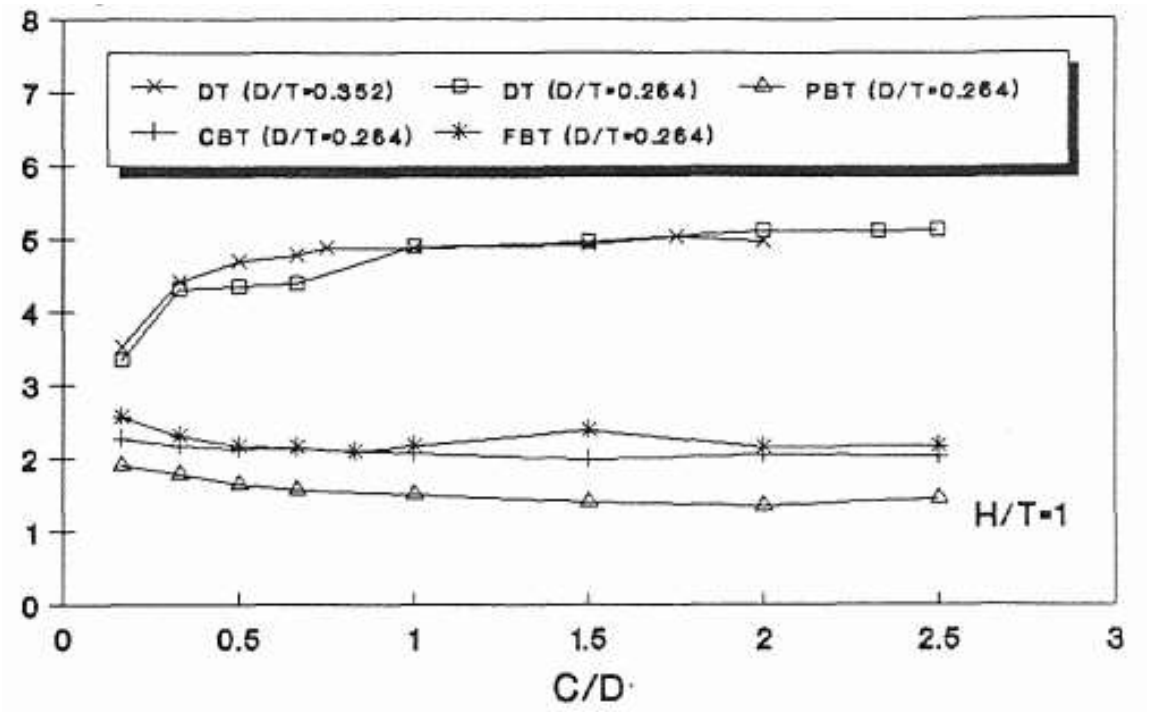

Figure 25 Effect of Clearance on Np[10]

3.Computational Fluid Dynamics (CFD)

3.1 Introduction

Computational fluid dynamics (CFD) is used to predict flow behavior and other associated phenomena through mathematical modelling and simulation using computer-based programs. Initially, CFD was used in the aerospace industry in the 1960s and because of the compatibility of CFD with other industrial processes and its ability to predict the flow behavior; it was extended to most other industries such as automobile, aircraft, and process and mixing industries.

CFD is able to predict the velocity profile, fluid flow directions, shear forces, local energy dissipation, power demand for the impeller, heat transfer coefficients, and local pressure distribution by solving the governing equations like equation of motion, continuity equation, and Naiver-Stoke equations simultaneously.

3.2 CFD code

The CFD code is dependent on numerical mathematics, where numerical algorithms are employed to solve the problem. The code consists of three main parts: the preprocessor, the solver, and the postprocessor. In the first phase, the system problem is defined. This includes the geometry of the system, fluid properties, grid generation, grid dependency, and boundary conditions. And this problem is transformed into an idealized and discretized computer model. In the solver, the actual computation is performed by the solver and in the solving phase, computational power is required. There are three types of solvers available varying in efficiency and capacity, which are finite difference, finite element, and spectral method. Finally, in the post-processing phase, the results obtained are analyzed and visualized.

3.3 Conservation law applicable to the system

Mass, momentum, and energy in the system is conserved. The governing equations of flow can be based on any applicable conservation laws of physics. The general format of these laws in a controlled volume is as follows.

$$\{\text{Rate of changes}\} = \{\text{Inlet}\} - \{\text{Outlet}\} + \{\text{Rate of source generation}\} \qquad (8)$$

3.4 Fluid flow regime

Understanding the fluid flow regime is very crucial for minimizing the operating cost. The fluid flow regime is classified into two types, which are laminar flow and turbulent flow. These flows are very important when it comes to design and operating costs. These flows will also determine the amount of energy required to maintain the desired fluid flow using fluid friction. The flow regime of the impeller is characterized as the impeller Reynold's number which is defined as.

$$Re = \frac{\rho N D^2}{\mu} \qquad (9)$$

Where ρ is the density in (kg/m3) of the fluid , N is the speed of the impeller in revolutions per second (rps) ,D is the diameter of the impeller in (m) and μ is the viscosity of the fluid in (Pa. s). If the Reynolds number is less than 10, then the flow regime is called laminar flow. If Re is greater than 10^4 then it is turbulent flow and in between them is called transient flow.

3.5 Mathematical model

In this model, both the gas and the liquid phases are treated as an interpenetrating continuum represented by a volume fraction at each point of the system. The continuity equation and the momentum equation are [18], [19], [20]

$$\frac{\partial(\alpha_i \rho_i)}{\partial t} + \nabla\left(\alpha_i \rho_i \overrightarrow{U_i}\right) = 0 \qquad (10)$$

Where α_i, ρ_i, and $\vec{U}$ are volume fraction, density, and velocity vector, respectively.

$$\frac{\partial(\alpha_i \rho_i \overrightarrow{U_i})}{\partial t} + \nabla\left(\alpha_i \rho_i \overrightarrow{U_i}\right) = -\alpha_i \nabla p + \nabla \tau_i + \alpha_i \rho \vec{g} + \vec{R}_{ij} + \vec{F}_i \qquad (11)$$

where ρ is density, $\vec{U}$ is the velocity vector, p is pressure and is shared by both the phases, τ_i is the stress-strain tensor because of viscosity and velocity fluctuations, $\vec{g}$ is gravity acceleration, $\vec{R}_{ij}$ is the interaction force between phases, and $\vec{F}_i$ is the effects of external force, turbulent dispersion force, virtual mass force and lift force.

3.5.1 Turbulence equation

The standard k- ω model was used to simulate the flow in a vessel(turbulent fluid flow) because k-ε model is more suitable when studying the free shear layers and the wake region, but standard k-ω model provides more accurate solutions in the boundary regions near the wall [18] [19]. There is also an improved version of the k-ω model called SST k-ω in which k-ε and k-ω models are automatically activated in the domain.

The transport equation for k

$$\frac{\partial}{\partial t}(\rho k) + \frac{\partial}{\partial t}(\rho k u_i) = \frac{\partial}{\partial x_j}\left[\left(\mu + \frac{\mu_t}{\sigma_k}\right)\frac{\partial k}{\partial x_j}\right] + G_k - Y_k + S_k \qquad (12)$$

The transport equation for ω

$$\frac{\partial}{\partial t}(\rho k) + \frac{\partial}{\partial t}(\rho \omega u_i) = \frac{\partial}{\partial x_j}\left[\left(\mu + \frac{\mu_t}{\sigma_k}\right)\frac{\partial k}{\partial x_j}\right] + G_\omega - Y_\omega + D_\omega + S_\omega \qquad (13)$$

Where, k represents turbulent kinetic energy , ω is the specific rate of dissipation , ε is the rate of dissipation of turbulent kinetic energy, G_k is generation of turbulent kinetic energy that arises due to mean velocity gradients, G_ω is generation of ω , Y_k and Y_ω represents as dissipation rate of k and ω due to turbulence, $\alpha_k$and α_ω are the turbulent Prandtl numbers for k and ω respectively , S_k and S_ω are source terms and D_ω is the cross-diffusion term.

3.5.2 Volume of fluid multiphase method (VOF)

The VOF multiphase method is adopted to simulate the mixing of water and air in the vessel. The VOF formulation is usually used to calculate the time-independent solution. But for the steady-state problems, it is possible to carry out the steady-state simulation and be able to provide a solution independently of the initial guess. In the case of the vortex formation system with a liquid-gas interface, the solution depends on the initial height of the liquid. Therefore, the simulation must be performed in the transient case [24].

The VOF formulation depends on the fact that two or more phases do not interpenetrating each other. For each control volume, the volume fractions of all phases must be total to unity. The fields for all variables and properties are shared by the phases and represent volume-averaged values, provided that the volume fraction of all phases is well known at every location. Thus, the variables and properties in any known cell are characteristic of either only one of the phases or a mixture of the phases, as it depends on the volume fraction values. In different words, if the q^{th} fluid's volume fraction within the cell is indicated as α_q , then the following three conditions are possible [24]

- $\alpha_q = 0$ The cell is empty (of the q^{th} fluid)
- $\alpha_q = 1$: The cell is full (of the q^{th} fluid)
- $0 < 1 < \alpha_q$: The cell contained interface between the q^{th} fluid and one or more other fluids.

Based on the local value of αq , the appropriate properties and variables are assigned to each control volume within the computational domain.

The tracking of the interface between the phases is done by solving a continuity equation for the volume fraction of one or more of the phases. For the q^{th} (fluid's volume fraction) phase, the equation is written as [24]

$$\frac{1}{\rho_q}\left[\frac{\partial}{\partial \mathrm{t}}(\alpha_q \rho_q) + \nabla(\alpha_q \rho_q \overrightarrow{v_q}) = S_{a_q} + \sum_{p=1}^{n}(m_{pq} - m_{qp})\right] \qquad (14)$$

where, m_{qp} is the mass transfer from phase q to phase p and m_{pq} is the rate of mass transfer from phase p to phase q . By default, the source term on the right-hand side of equation S_{a_q} is zero, but can specify a constant or user-defined mass source for each phase.

The volume fraction equation will not be solved for the primary phase; the primary-phase volume fraction will be computed based on the following constraint:

$$\sum_{p=1}^{n} \alpha_q = 1 \qquad (15)$$

The properties appearing in the transport equations are determined by the presence of the component phases in each control volume. In a two-phase system, for example, if the phases are represented by subscripts 1 and 2, and the mixture density in each cell is given by [24]

$$\rho = \alpha_2 \rho_2 + (1 - \alpha_2)\rho_2 \qquad (16)$$

In general, for n phase system, the volume-fraction averaged density takes on the following form.

$$\rho = \sum \alpha_q \rho_q \qquad (17)$$

All other properties (e.g., viscosity) are also computed in this manner.

3.6 Vessel configuration

Flat-bottom baffled stirred vessel with an inner diameter (D) of 296 mm and a thickness of the wall (t) of 5 mm. Furthermore, an impeller with diagonally rounded blades is used with an outer diameter (d) of 106.2 mm and a height of the impeller (b) of 133 mm. The impeller off bottom clearance(C) or distance between impeller to flat bottom is 51 mm .The vessel was fitted with four vertical equally placed baffles with width(W) 30mm and thickness (s) 2 mm.The initial height of the liquid was set as 296mm(H=D) and then liquid decreases as shown in *table.3* to study the flow and power consumption changes of impeller. In this study, five different impeller rotational speeds are used, which are 50 rpm, 100 rpm, 150 rpm, 200 rpm , 300 rpm. The geometry of the system is seen in *Figure 26*.

Table 3 Different liquid height

H=D	0.75D	0.6D	0.5D	0.4D	Liquid height above 2mm of the impeller
296 mm	222mm	177. 6 mm	148 mm	118.4 mm	87 mm

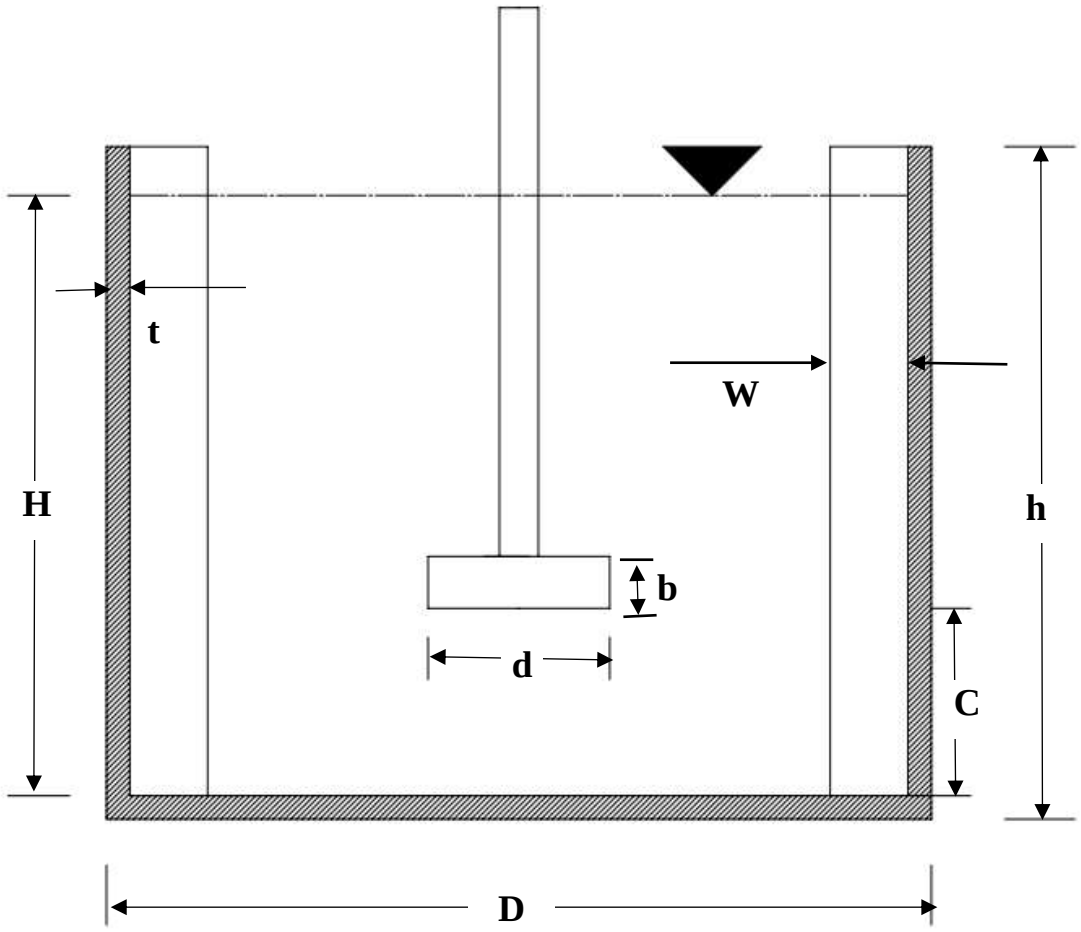

Figure 26 Geometry of the system

3.7 Design modeler

The design part of the 3D geometry was carried out in solid work, and then the design file was converted into the step file for further process. Then the step file is mounted in the ANSYS workbench. Then, to perform the CFD analysis, the mixing tank is filled with fluid. To fill the fluid in the tank, the free surface of the tank must be covered as shown in *Figure 27.* After the free surface is covered, the vessel is filled with the fluid, as shown in *Figure 28.*

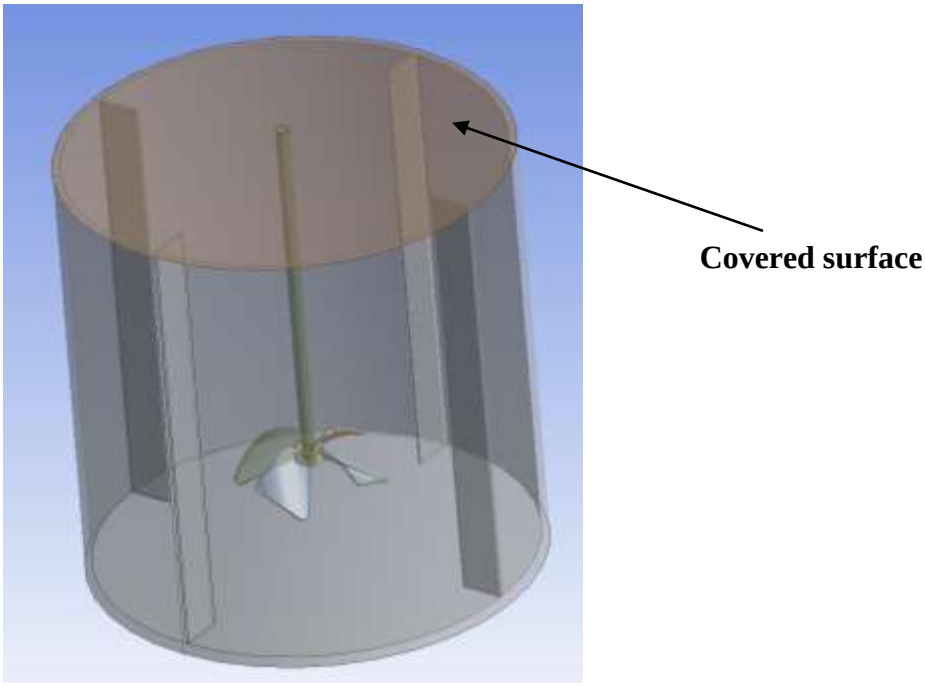

Figure 27 Mixing tank with covered surface

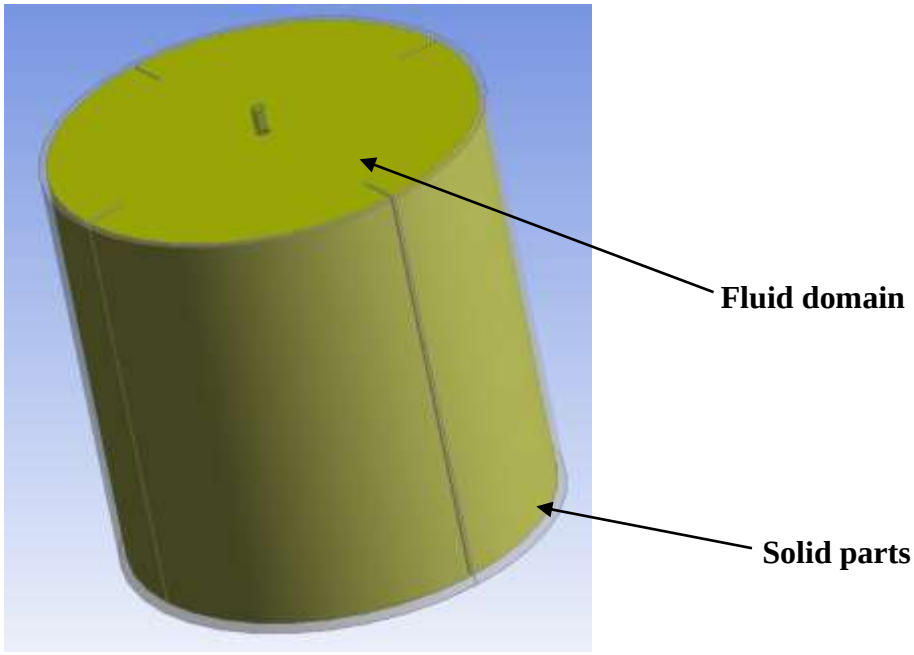

Figure 28 Mixing tank is filled with fluid or created fluid domain

Now, the solid parts such as mixing tank, shaft, and impeller are removed in order to perform the numerical analysis, as shown in *Figure.29* using the boolem operation called substract.

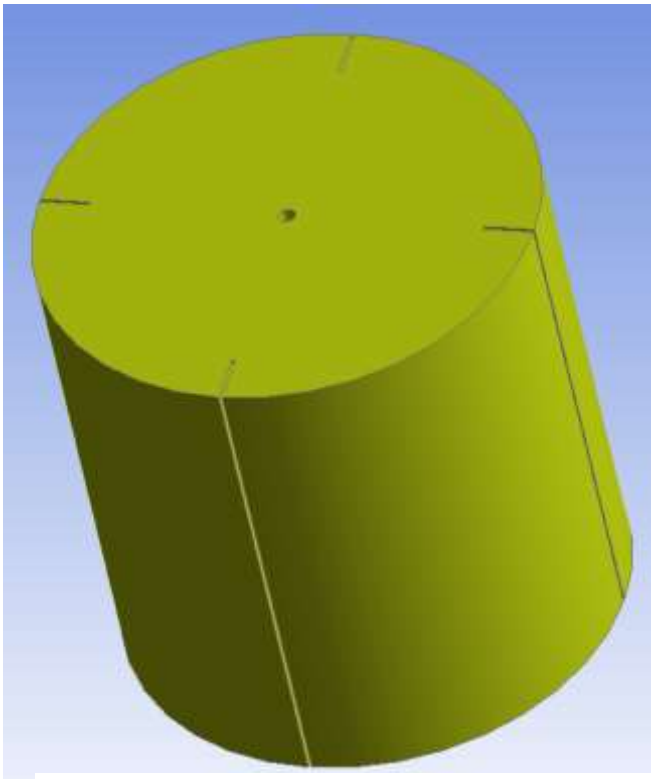

Figure 29 Fluid domain without any solid parts

To adopt the MRF method, the fluid domain is sliced into a rotating zone by creating a cylinder inside the fluid domain with radius 99.65mm and height 50.82mm using the option called primitives in the create section. The created rotating zone can be seen in *Figure 30.*

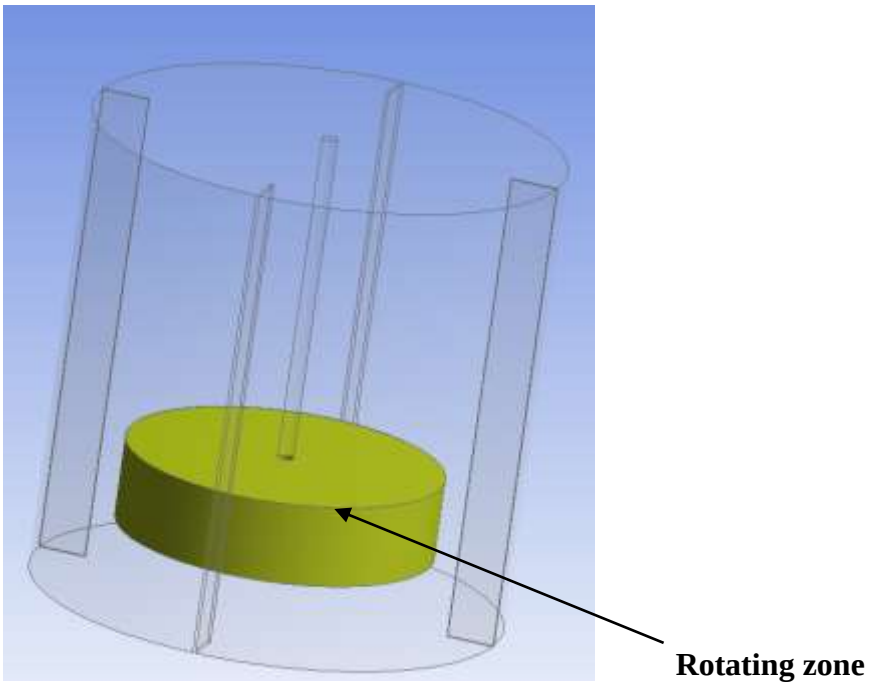

Figure 30 Mixing tank with rotating zone

3.8 Rotating reference frame model

In this approach [25],the rotating frame in the entire model is solved by the momentum equation. In other words, the frame is considered stationary but inertial. Therefore, the additional acceleration term incorporates the equation of motion due to the transformation of stationary to rotating reference frame, as shown in *Figure 31*.

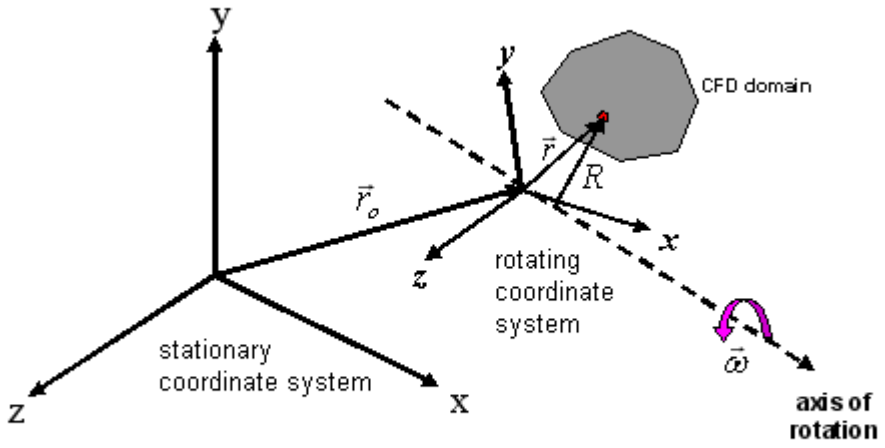

Figure 31 Rotating reference frame with angular velocity (ω) [25]

Consider the CFD domain rotating around an axis with unit vector $\vec{a}$ and an angular velocity magnitude of (ω), the rotation vector is defined as

$$\overrightarrow{\omega} = \omega\vec{a} \qquad (18)$$

The computational domain for the CFD problem is defined with respect to the rotating frame such that an arbitrary point in the CFD domain is located by a position vector $\vec{r}$ from the origin of the rotating frame. The fluid velocities can be transformed from the stationary frame to the rotating frame using the following relation[25]

$$\overrightarrow{u_r} = \vec{u} - \overrightarrow{u_{wr}} \qquad (19)$$

where

$$\overrightarrow{u_{wr}} = \vec{\omega} \times \vec{r} \qquad (20)$$

In the above, $\overrightarrow{u_r}$ is the relative velocity (the velocity viewed from the rotating frame), $\vec{u}$ is the absolute velocity (the velocity viewed from the stationary frame), and $\overrightarrow{u_{wr}}$ is the whirl velocity (the velocity due to the moving frame)

Continuity equation for rotating frame :

$$\frac{\partial\rho}{\partial t} = -(\nabla.\partial\overrightarrow{u_r}) \qquad (21)$$

Momentum equation for rotating frame

$$\frac{\partial \rho \vec{u}}{\partial t} = -(\nabla . \rho \overrightarrow{u_r} \vec{u}) - \rho(\vec{\omega} \times \vec{u}) - \nabla p - (\nabla \bar{\tau}) + \rho \vec{g} + \vec{F} \quad (22)$$

where the Coriolis and centripetal accelerations are considered in $(\vec{\omega} \times \vec{u})$

3.9 Multiple reference frame (MRF)

In this study the MRF approach is used to simulate the rotating part impeller and shaft shown in *Figure 32. The* MRF model is the simplest of the two approaches for multiple zones. It is a steady-state approximation where the cell zone moves at different or the same rotational speed. The flow in each cell zone is solved by the governing moving reference frame equations. The stationary zone is solved by stationary equations, and the rotating or moving cell zone is solved by moving reference equations, and information is exchanged at the interface. The properties of the flow at the interface between the rotating and stationary zones are translated directly into MRF. In MRF approach, there is no relative motion between adjacent zones with respect to the moving zone, the grid is fixed for computation. This is analogous to freezing the motion of the moving or rotating part in a specific position and observing the flow field with the rotor in that position. So MRF is also referred to as the "frozen rotor approach."

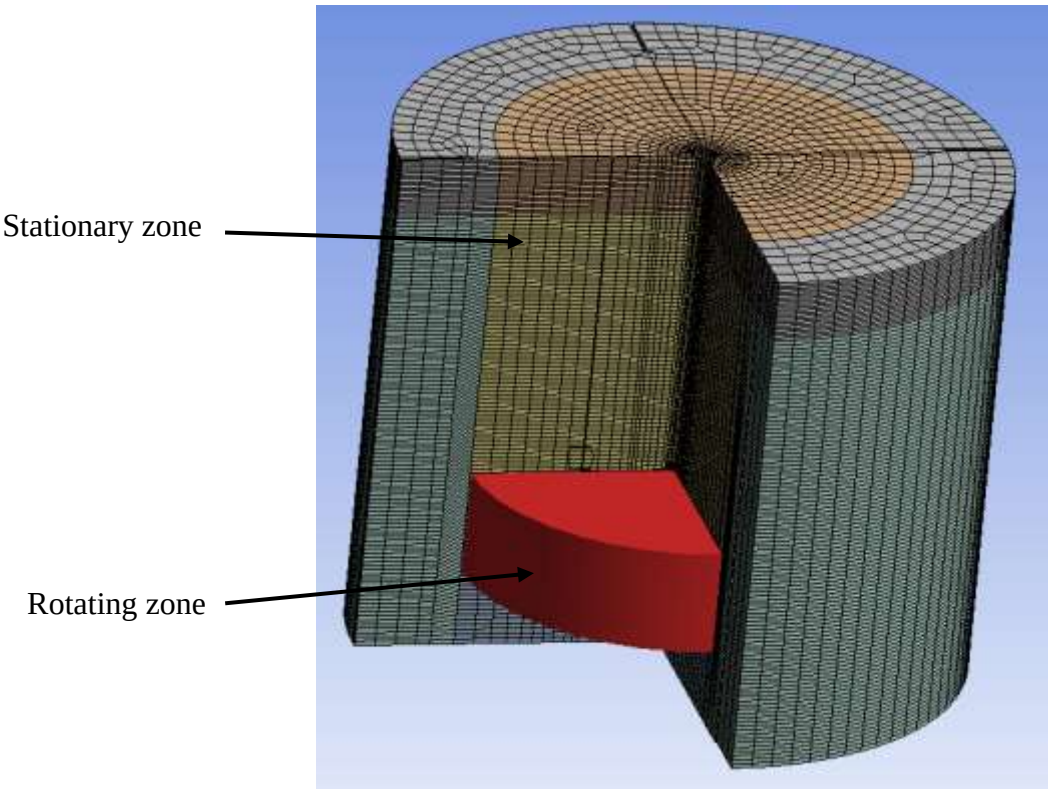

Figure 32 Multiple cell zones to mimic the impeller motion in a quarter of baffled mixing tank

3.10 Mesh Generation

Meshing is also known as mesh generation; in this process, a two-dimensional or three-dimensional grid is generated by dividing the complex geometries into the elements that can be used to discretize the domain. A mesh can be generated in different shapes and sizes, see *Figures 33 &34.*Shapes matter when it comes to dividing the domain from subdomain for parallel processing, and size of the element is important when it comes to sharp gradient of the entity.

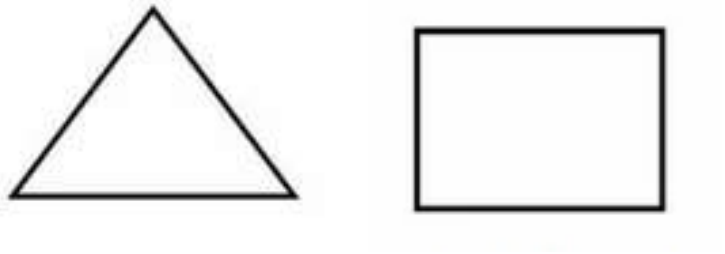

Figure 33 2D cell types, from left to right : triangle , quadrilateral

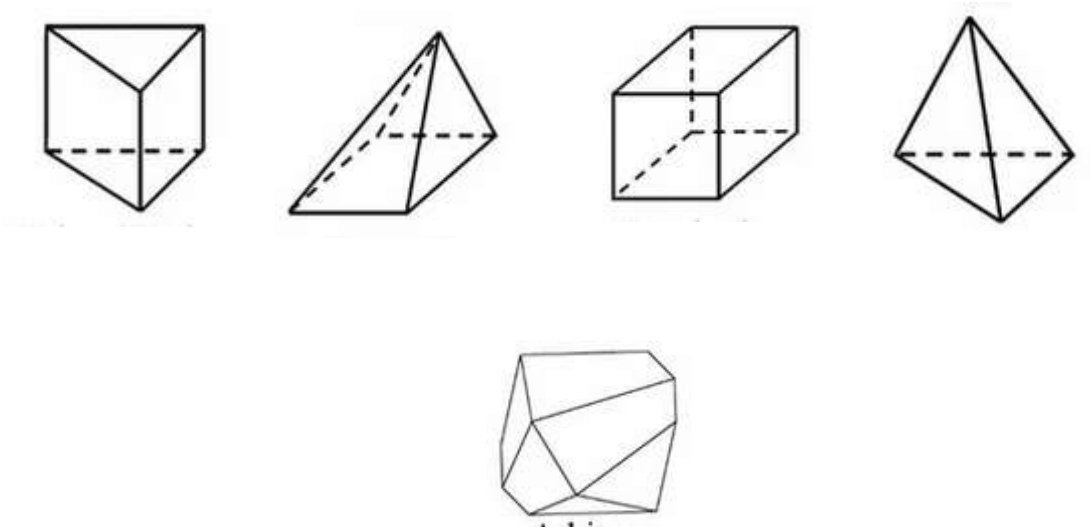

Figure 34 3D cell types, from left to right: Tetrahedron, Pyramid, Hexahedron, Prism, Polyhedron

Creating the most appropriate mesh is the foundation for CFD simulation. This is because the mesh greatly influences the accuracy, convergence, and speed of the simulation. Skewness quality also greatly influences the accuracy of the result and the convergence of the simulation. The skewness quality indicates how much error there is in a single cell, and the quality range is from 0-1. *Figure.35* shows that elements have different skewness. And the mesh processing in ANSYS is shown in *Figure.36.*

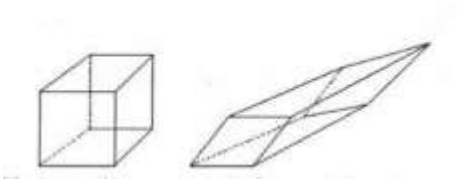

Figure 35 Elements with different skewness, left : low skewness, right : high skewness , right: high skewness

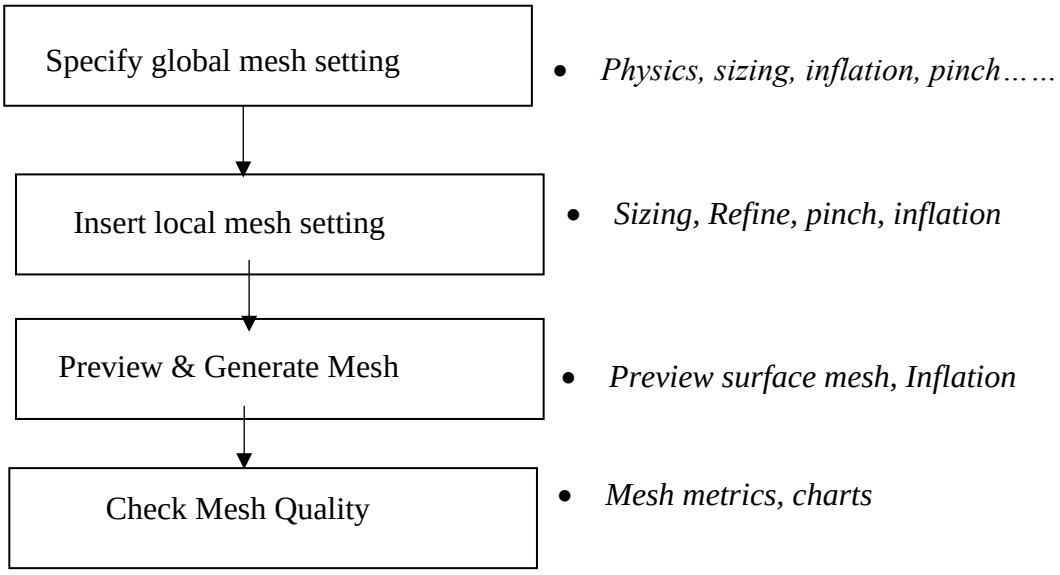

Figure 36 Mesh processing in ANSYS mesh[27]

In this study, the unstructured mesh tetrahedron is generated first, as shown in *Figure 37*. To obtain good mesh quality, the structured mesh hexahedron is generated by slicing the geometry in the XY plane in the design modeler is shown in *Figure 38*. So that hex sweep mesh is enabled in order to get a structured mesh, they are shown in *Figure 39*. On the other hand, the unstructured mesh is generated for the impeller. Since it has many sharp edges and corners, the proximity and curvature options are used to generate the unstructured tetrahedron mesh. The skewness quality for the mesh is 0.88 and the minimum orthogonal quality is 0.11. The number of mesh elements is 400000 to 500000.

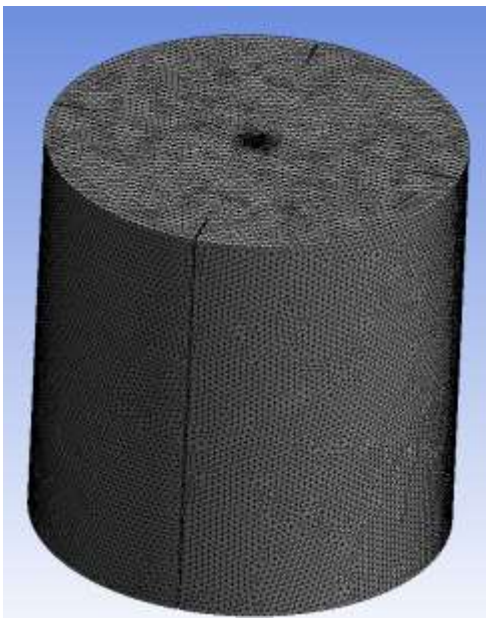

Figure 37 Unstructured or Tetrahedron mesh

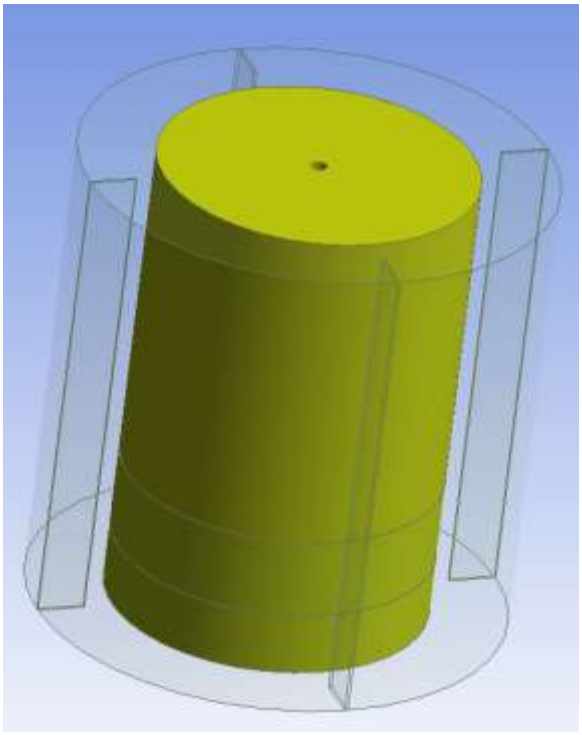

Figure 38 Sliced geometry

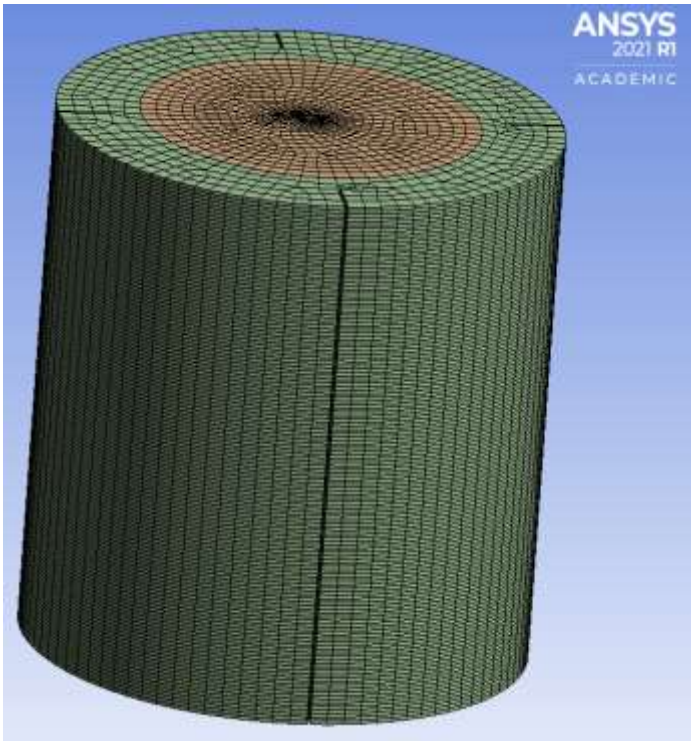

Figure 39 Structured or hexagonal mesh

After the mesh is generated, the name selection is made based on the region that is impeller, shaft, wall, surface, inner domain, outer domain and air domain as shown in *Figure 40.*

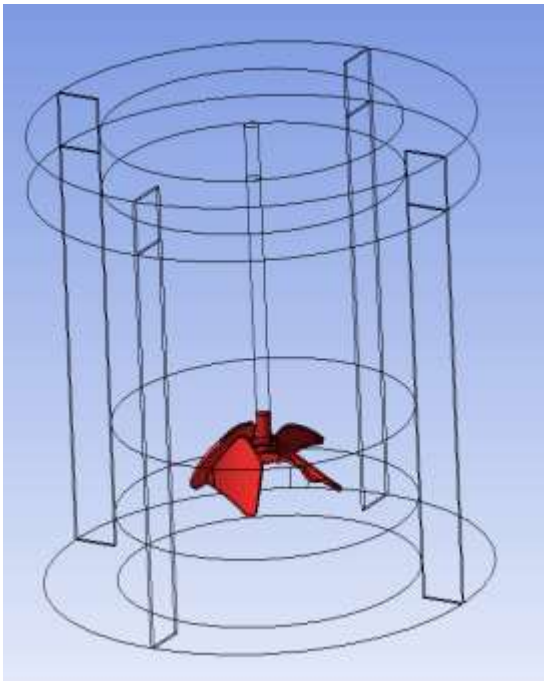

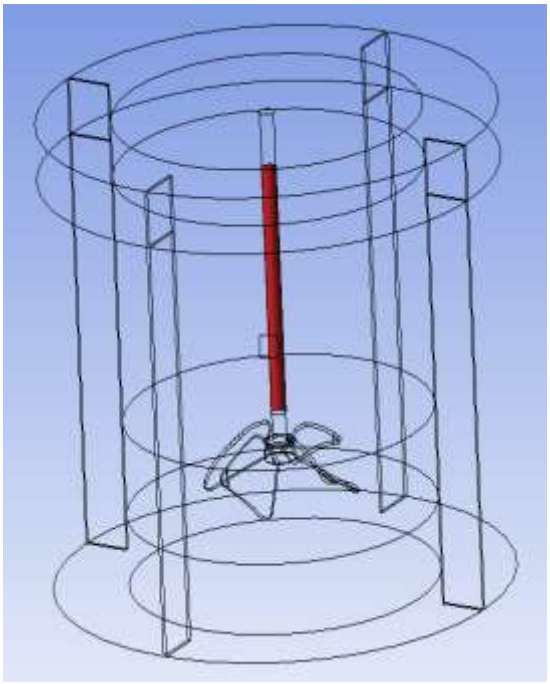

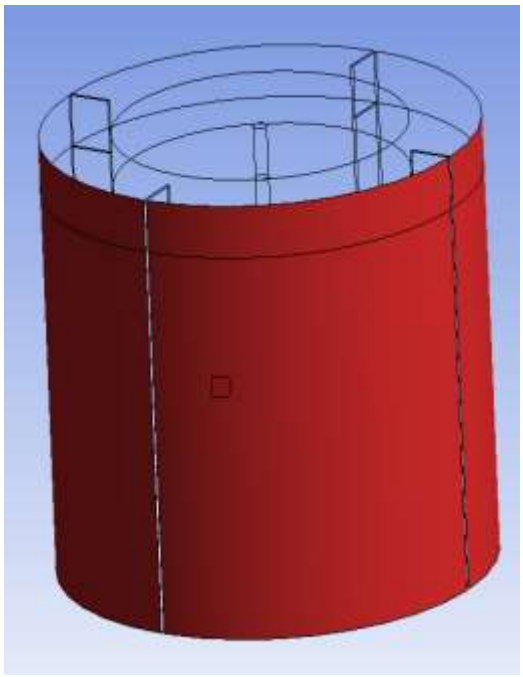

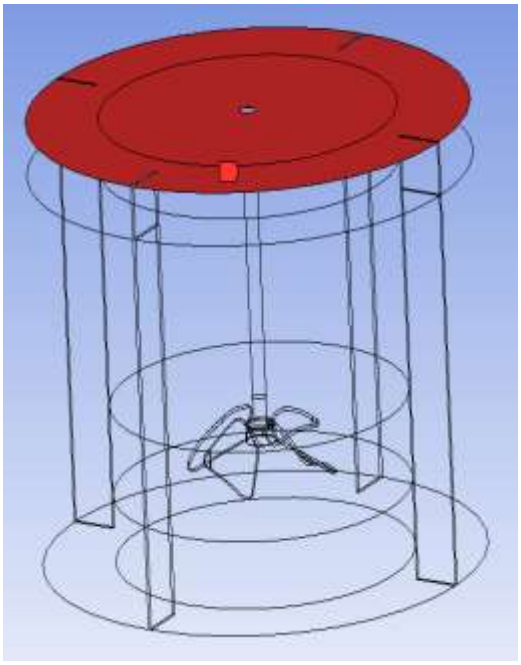

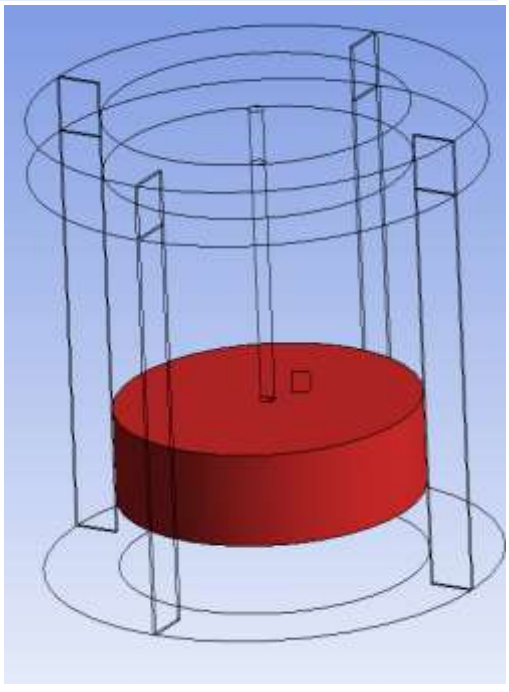

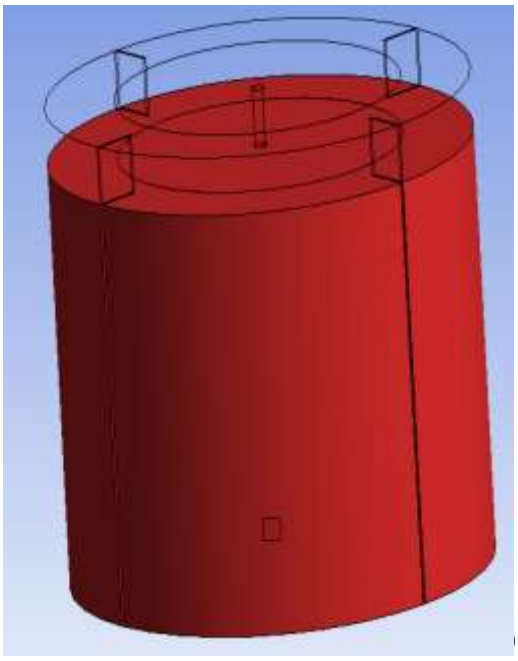

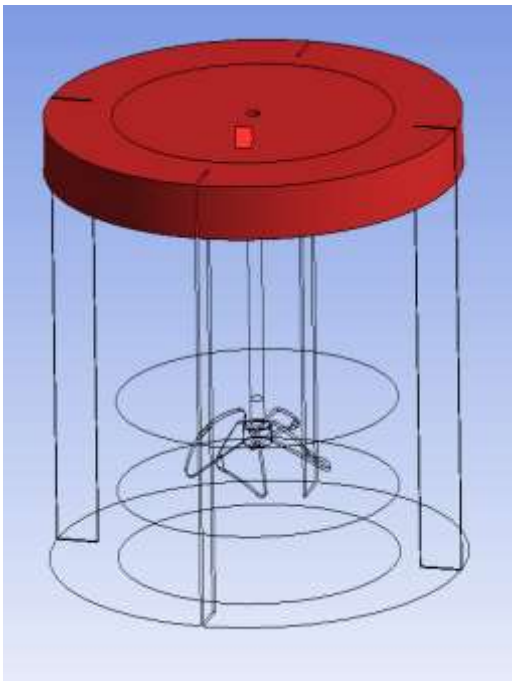

Figure 40 Name selection according to the region : from left to right : impeller,shaft,wall, surface, inner domain, outer domain and air domain

3.11 Specifying material physical properties and units

Once the mesh is generated , it is then implemented in Fluent solver where we set the desired parameter according to our requirements. First, the unit of the rotational speed impeller is chosen as revolution per minute (Rpm) and the physical properties of all phases or the properties of the working fluids involved in partial differential equations should be defined properly as shown in *Figure.41&42*, because the final results are highly dependent on these properties of the material. The working fluid in this study is water with density (ρ) 997.256 kg/m^3 and dynamic viscosity (μ) 0.000911 $kg/\,m\,s$ at 24 ° C and air with density (ρ) 1.225 kg/m^3 and dynamic viscosity (μ) 1.7894e-05 $kg/\,m\,s$.

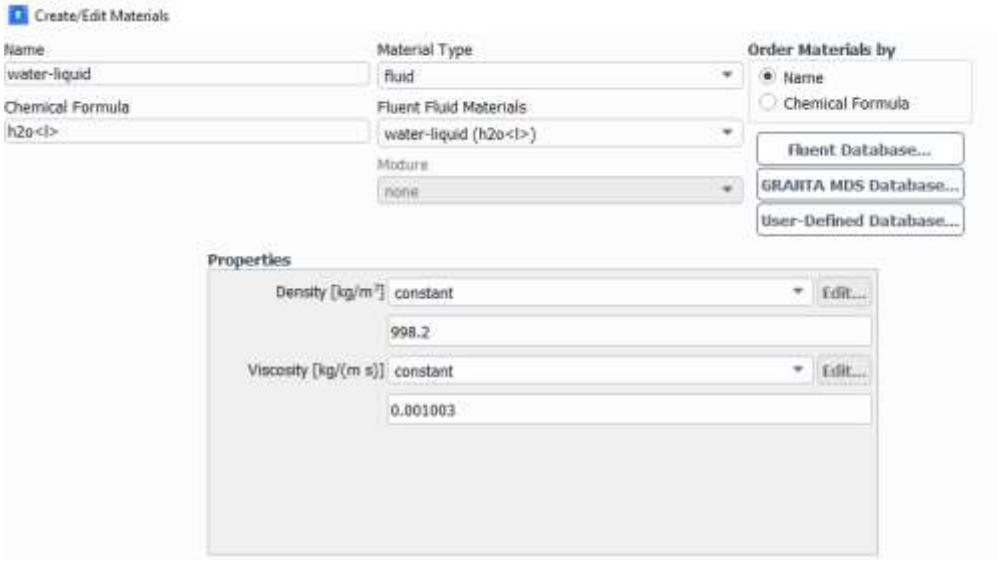

Figure 41 Fluid material : water-liquid (H20)

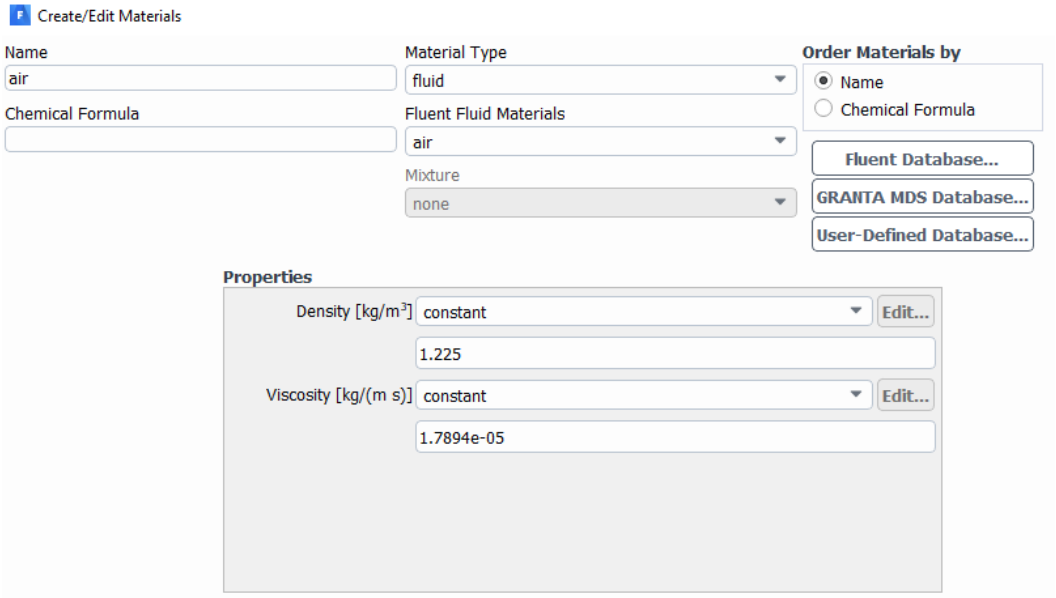

Figure 42 Fluid material : Air(O2)

3.12 Cell zone conditions

In the cell zone the mesh consists of a large number of finite-volume or cells, and these cells are grouped with one or more cells, and they are called the cell zone. In this study, there are three cell zones, the inner domain, the outer domain and the air domain, shown in *Figure.43* where the inner domain is a rotating part and the outer domain and the air domain is a stationary part. Since the inner domain is a rotational part, the rotational speed of the impeller is specified in this zone, as shown in *Figure 44.* Furthermore, initially, the outer domain and inner domain are filled with water and the air domain is filled with air. The air domain is created as a result of the vortex formation during operation or mixing. During the vortex formation, some volume of the tank will be without any water. So, to fill this empty volume ,the air domain is created.

.

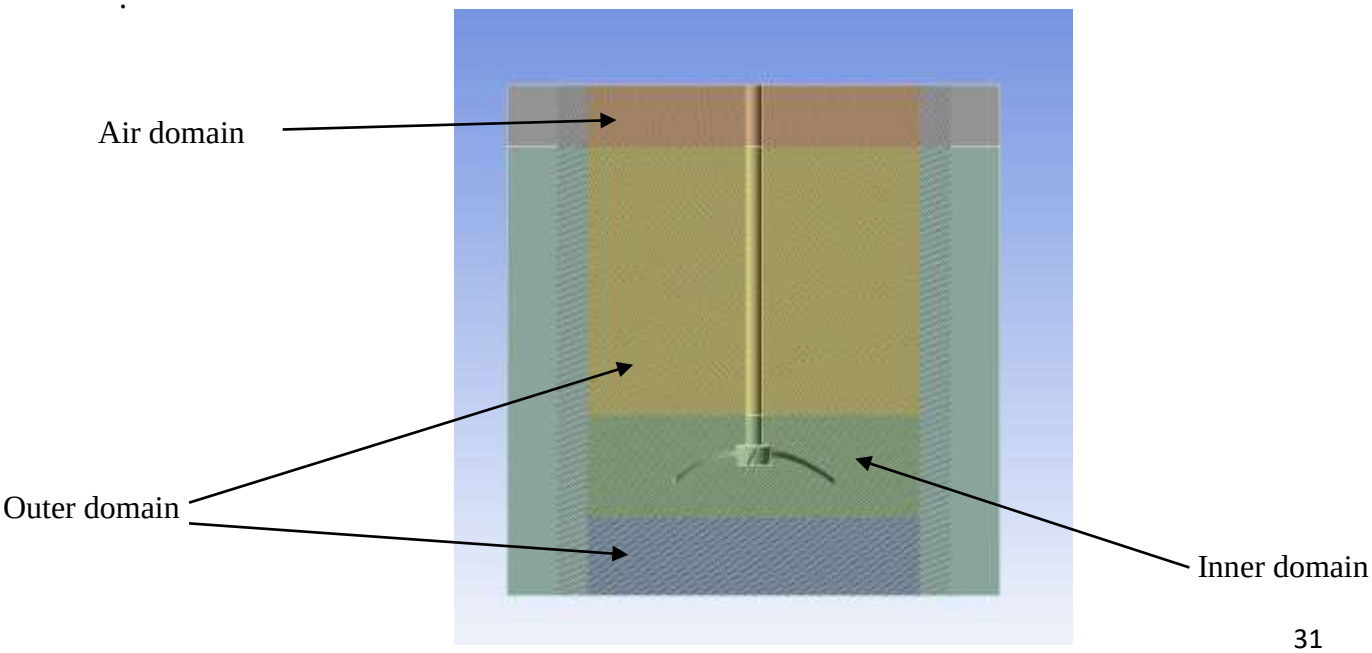

Figure 43 Cell zone conditions

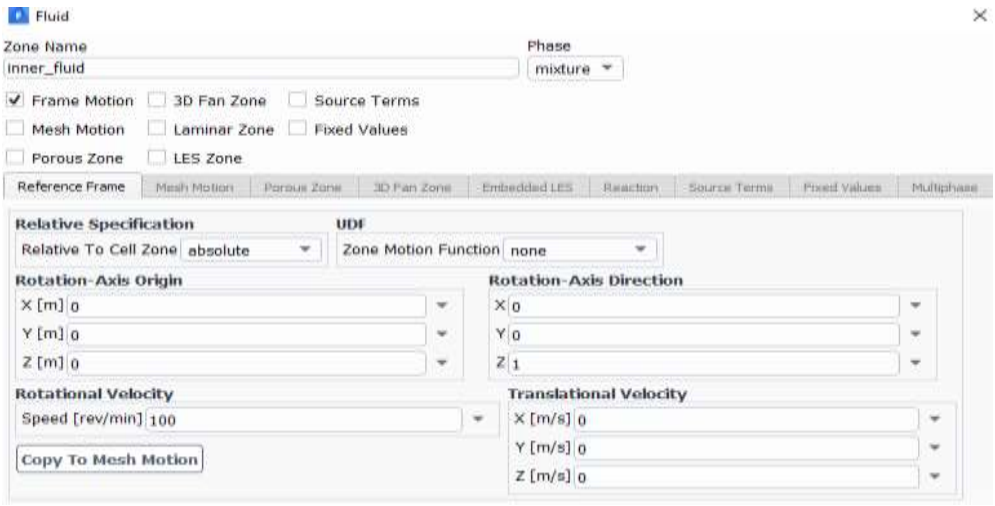

Figure 44 Cell zone condition for inner domain

3.13 Implementation of boundary conditions

To define a problem that results in a unique solution, we need to specify information on the flow variable at domain boundaries like specifying fluxes of mass, momentum, energy, etc. on the domain boundaries. So, it is very important to understand and specify them correctly because they force the governing equation to follow the problem specifications. Poorly defined boundary conditions cause an error in the final solution. Defining boundary conditions are based on geometry, available data on boundary conditions, and numerical considerations. The most commonly used boundary conditions are listed below.

- Wall
- Symmetry
- Inlet
- Outlet
- Prescribed pressure
- Periodicity or cyclic boundary condition

Geometry-related boundary conditions are classified into two categories, which are

- Stationary boundaries
- Rotating or moving boundaries

In this study, the geometry has three boundary conditions, which are wall, symmetry or pressure outlet, and rotating boundaries as shown in *Figure 45. The* boundary conditions for the free surface are symmetry. Since both the impeller and the shaft will be moving parts, the boundary condition is given as rotating boundaries and all baffles and walls are assigned as stationary boundaries.

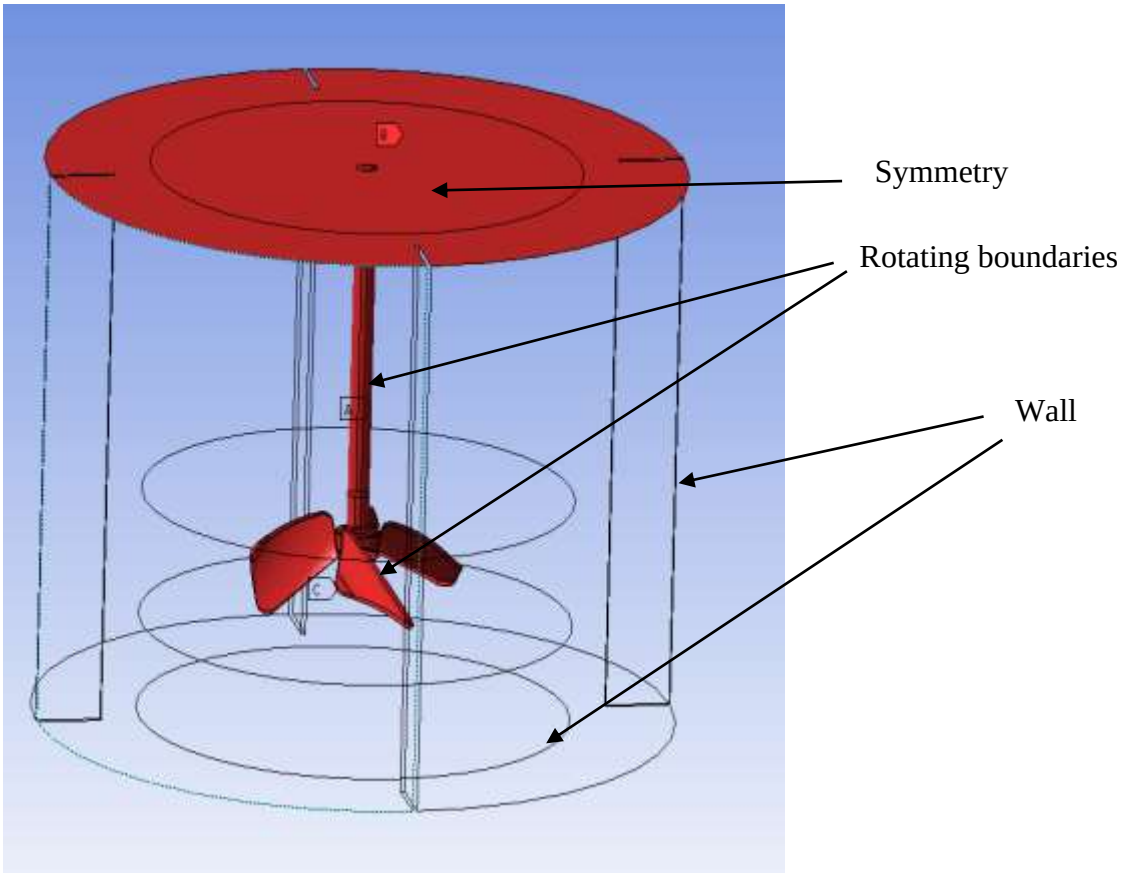

Figure 45 Boundary conditions

3.13.1 Stationary Boundaries

The typical stationary boundaries in the mixing tanks are walls and baffles where no slip-boundary conditions are applied to represent the surface. In such a case, the velocity for all the components is equal to zero.

3.13.2 Rotating or moving boundaries

Reciprocating pistons, pumps, and impellers are the example for the rotating boundaries. This type of boundary conditions is time-dependent and computationally costly in terms of time. In this study, the rotational speed is specified on the rotating boundary impeller and shaft.

3.14 Solution method of discretized equation

The nonlinear algebraic equations are the result of a discretization process which can be solved by two methods, the coupled method and the segregated method.

Coupled solution method: The coupled approach forms a single large system of equations that solves all the unknowns in each cell at once with a single iteration.

Segregated solution method : On the other hand, the segregated method will not solve all the unknowns at once. Instead, it subdivides the problem into two or more segregated steps.

The coupled solution method is more robust and requires more computational time compared to the segregated approach [17]. So, in this study, the coupled approach is used to get the solution.

3.14.1 Pressure velocity coupling

For incompressible fluids , their solutions are pressure-based but in the density-based solver, pressure-based is quite tricky. Therefore, in this study a pressure-based solver is adopted. There are several algorithms offered in the pressure-based solver which are listed below.

- Semi-implicit method for pressure-linked equations (SIMPLE)
- Semi-implicit method for pressure-linked equations consistent (SIMPLEC)
- Pressure implicit with splitting of operators (PISO)

So, in this study, the PISO algorithm is adopted since it is much faster compared to SIMPLE and SIMPLEC.

3.15 Discretization of partial differential equations

Once the cell or mesh is generated, an approximation of the transport equation should be applied to the discrete subdomains to predict the changes in entity within the entire domain of interest. The finite-volume method discretizes the differential equation based on truncated Taylor series spatially. Other alternative methods to solve the Navier-Stokes equations could be finite difference and finite element methods [17].

Temporal discretization is classified into two main methods: Explicit and implicit approaches.

- Explicit approach is that the solver method is used to find the solution of the time dependent by considering the solution of the system only at current time step. However, it is unstable or stable only for small integration time steps and is more likely to diverge.
- The implicit approach is similar to the explicit method, but it finds the solution of the system by predicting the future time step. It is more stable, but more iteration is necessary.

The pressure gradient is predicted by different schemes, which are listed below.

- Standard
- Linear
- PRESTO
- Second order scheme
- Body force weighted

Momentum interpolation schemes are divided into

- First order Upwind
- Second order upwind
- QUICK
- Third order MUSCL

In this study, initially the first-order discretization scheme was chosen to ensure convergence, and then it was switched to the second-order discretization scheme. Then PRESTO is chosen as the pressure gradient. An implicit scheme was also chosen to discretize the differential equations.

3.16 Residual and convergence

Since the numerical solution initially starts with a guess, there will be residual.so it is solved in an iterative process. The iterative process will stop once the residual tolerance is reached. This tolerance depends on the problem of the system or the desire of the user. In this study, the residual tolerance criteria for continuity are set as 1^{-05}.Residual curves are shown in *Figure 46.*

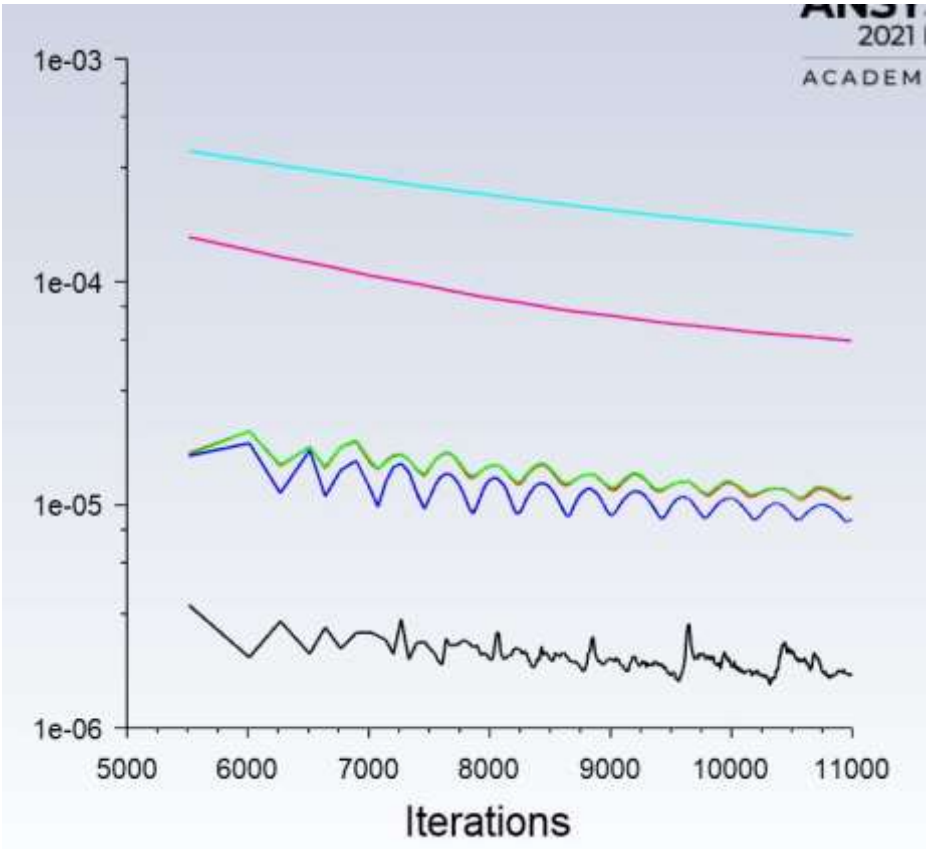

Figure 46 Residual monitoring of this study in which continuity-scaled residuals have been decreased until 1^(-05).

Generally, scaled residuals are used to monitor the convergence of the solution. On the other hand, choosing the proper time step size also has an impact on the solution accuracy and convergence, because the wrong time step size leads to an error in the final solution and difficulties in convergence. In this study, the time step size 0.0001, the number of time steps 10,000 and the maximum iteration 20 is adopted.

3.17 CFD Summary

The solution was performed in ANSYS 2021 R1. The solver was set according to Table 4

Table 4 Fluent solver setup for mixing tank

Number of mesh elements	400000 - 500000
Multiphase model	Volume of fluid (VOF)
Turbulence model	SST-K-Omega
Cell-zones	Inner domain, outer domain and air domain
Boundary Conditions	• Impeller and shaft are assigned as rotating boundaries • The baffle and wall are assigned as stationary boundaries. • The surface or vessel surface is assigned as symmetry.
Pressure-velocity coupling scheme	Pressure implicit with splitting of operators (PISO)
Discretization - Pressure	PRESTO
Discretization – momentum	Second-order upwind
Discretization – VOF	Compressive
Discretization - Turbulent kinetic energy	Second-order upwind
Discretization - Turbulent Dissipation Rate	Second-order upwind
Under relaxation factor	Momentum is reduced from 0.7 to 0.3 to achieve faster convergence.
Residuals	1^{-05}.
Time-Step Size	0.0001
Number of time steps	10,000
Maximum iteration	20
Computational time	1 day

4.Results and discussion

In this chapter, CFD results are compared with experimental data. It starts with the qualitative and quantitative validation of the CFD model and will be followed by a discussion on the results.

4.1 Shaft torque

CFD computes the total moment by summing the cross product of the pressure and viscous force vectors for each face with the moment vector $\overrightarrow{r_{AB}}$, which is the vector from the impeller center (A) to the force origin shaft center (B) is shown in *Figure 47*.

The equation for the total moment vector is

$$\overrightarrow{M_A} = \overrightarrow{r_{AB}} \times \overrightarrow{F_P} + \overrightarrow{r_{AB}} \times \overrightarrow{F_V} \qquad (23)$$

Where, $\overrightarrow{M_A}$ is total moment, $\overrightarrow{r_{AB}}$ is moment vector, $\overrightarrow{F_P}$ Pressure force vector and $\overrightarrow{F_V}$ is viscous force vector.The first and second term in the summation represents pressure moment and viscous moment[26].

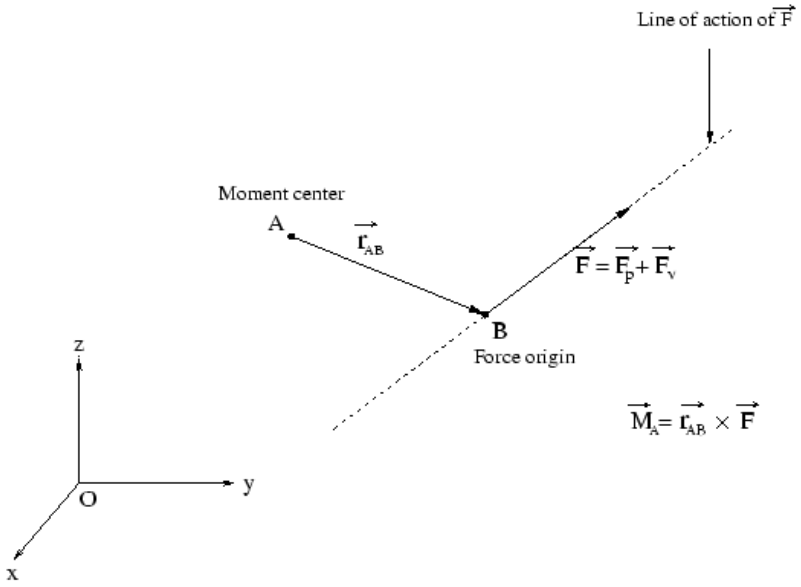

Figure 47 Moment About a Specified Moment Centre[26]

The direction of the total moment vector follows the right-hand rule for cross-products. Moment coefficients are calculated for each of the selected wall zones, together with the actual components of the pressure, viscous and total moments using the reference values. The moment coefficient is defined as the moment divided by $\frac{1}{2}\rho v^2 AL$, where ρ, v, A, and L are the density, velocity, area and length. The coefficient values for the individual wall zones are also summed to produce the net values of the pressure, viscosity, and total moments and coefficients for all the selected wall zones [26].

Furthermore, the moments along a specified axis are computed. These moments, also known as torques , are defined as the dot product of a unit vector in the direction of the specified axis and the individual and net values of the pressure, viscous, and total moments and coefficients. To reduce round-off error, a reference pressure is used to normalize the cell pressure for computation of the pressure force. For example, the net pressure force vector, acting on a wall zone, is computed as the sum of the vectors of the individual force vectors for each cell face as follows [26].

$$\overrightarrow{F_P} = \sum_{i=1}^{n}(P - P_{ref})A\vec{n} = \sum_{i=1}^{n} PA\vec{n} - P_{ref}\sum_{i=1}^{n} A\vec{n} \qquad (24)$$

Where, n is number of faces , A is the area of faces , P_{ref} is reference pressure and $\vec{n}$ is unit normal to face.

The torque calculated from the CFD and the experiment for the different liquid heights with respective rotational speeds is shown in *Figure 48-53*. The calculated torque, power number, and power consumption from the experimentally measured data are shown in further text.

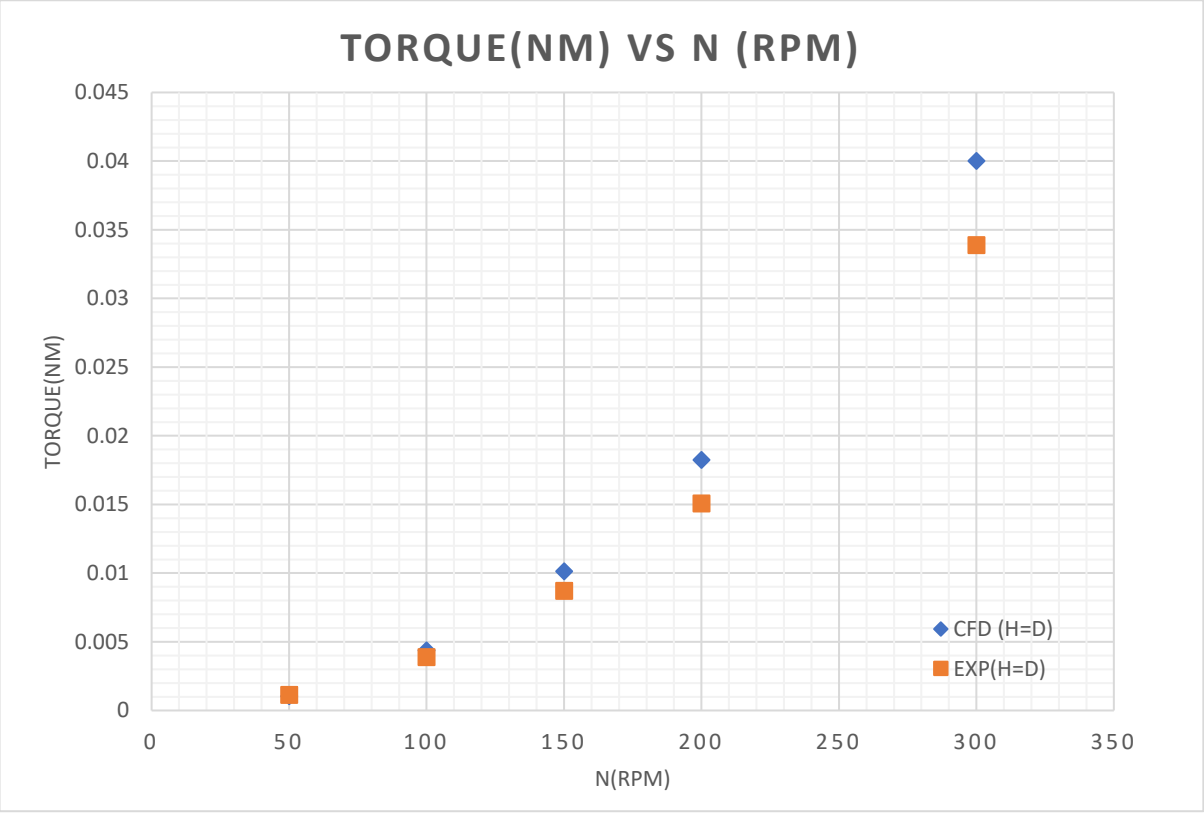

Figure 48 Comparison of torque from experiment and CFD at liquid height H=D

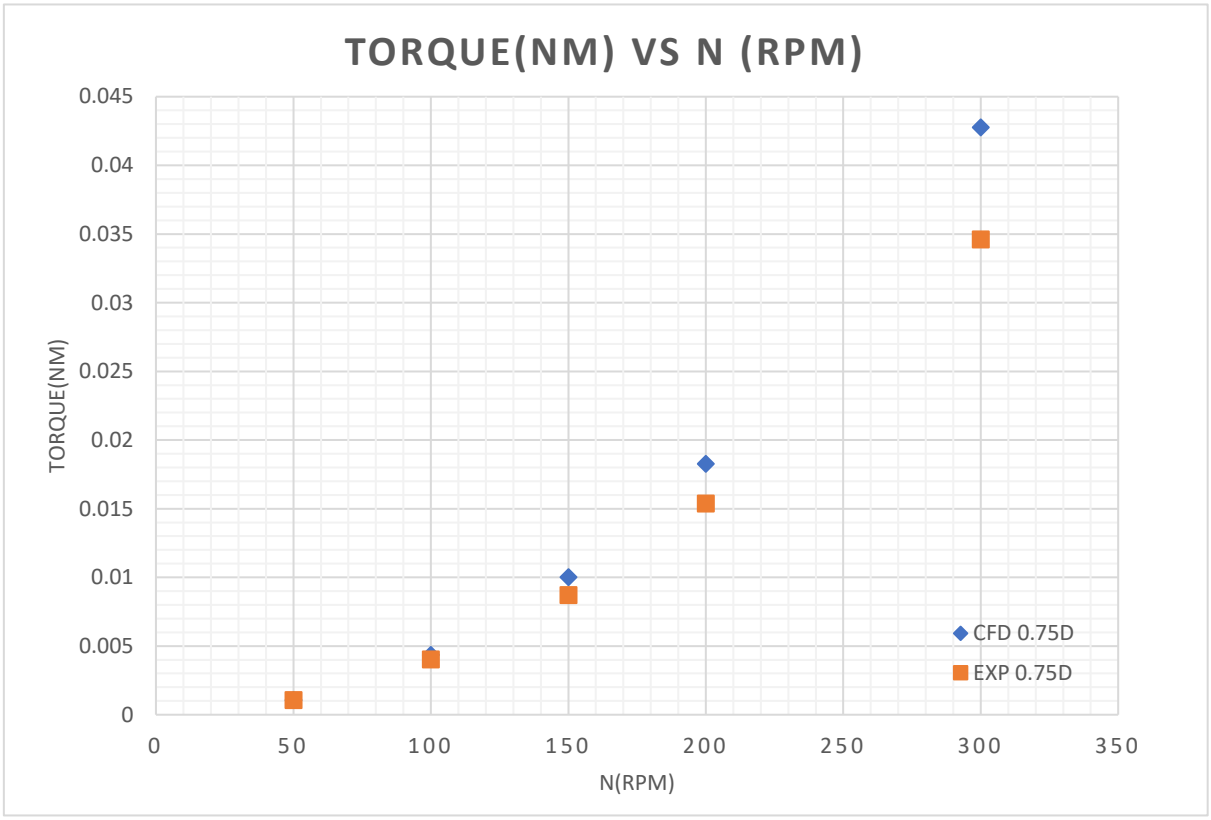

Figure 49 Comparison of torque from experiment and CFD at liquid height 0.75D

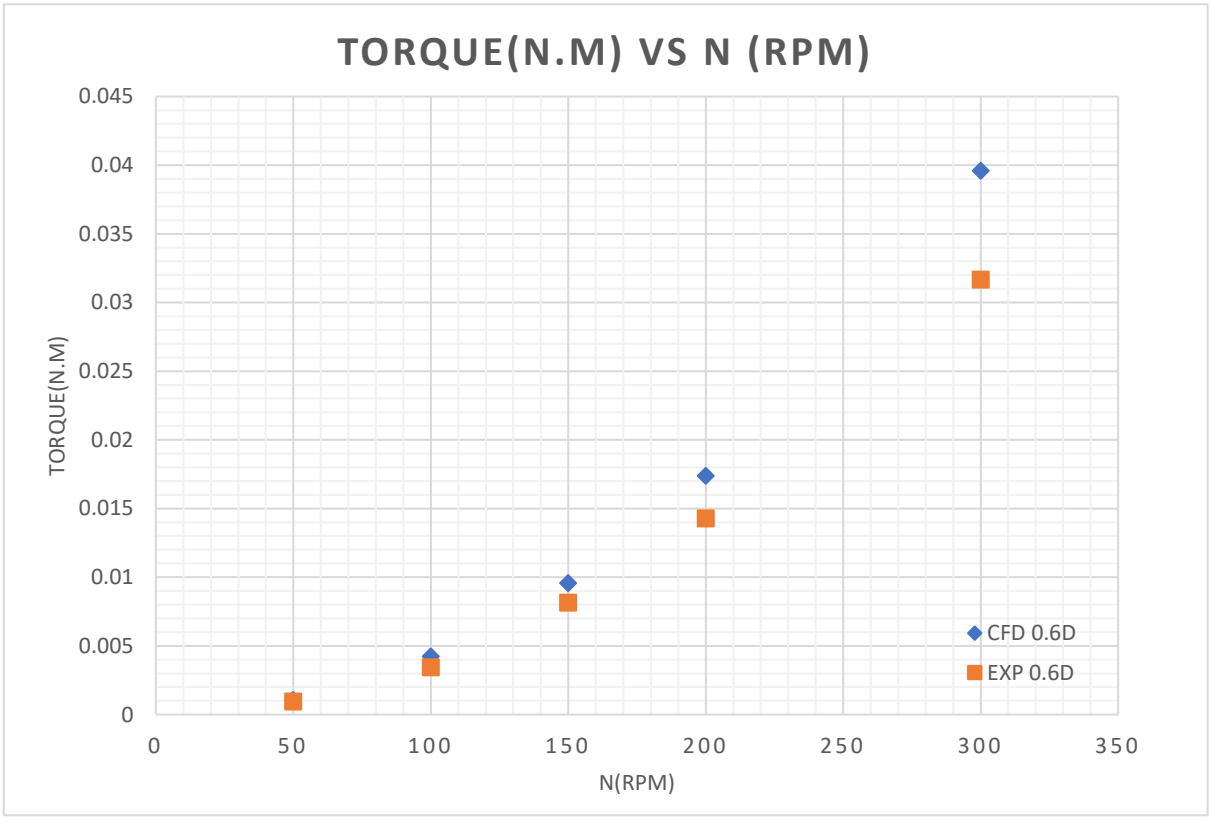

Figure 50 Comparison of torque from experiment and CFD at liquid height 0.6D

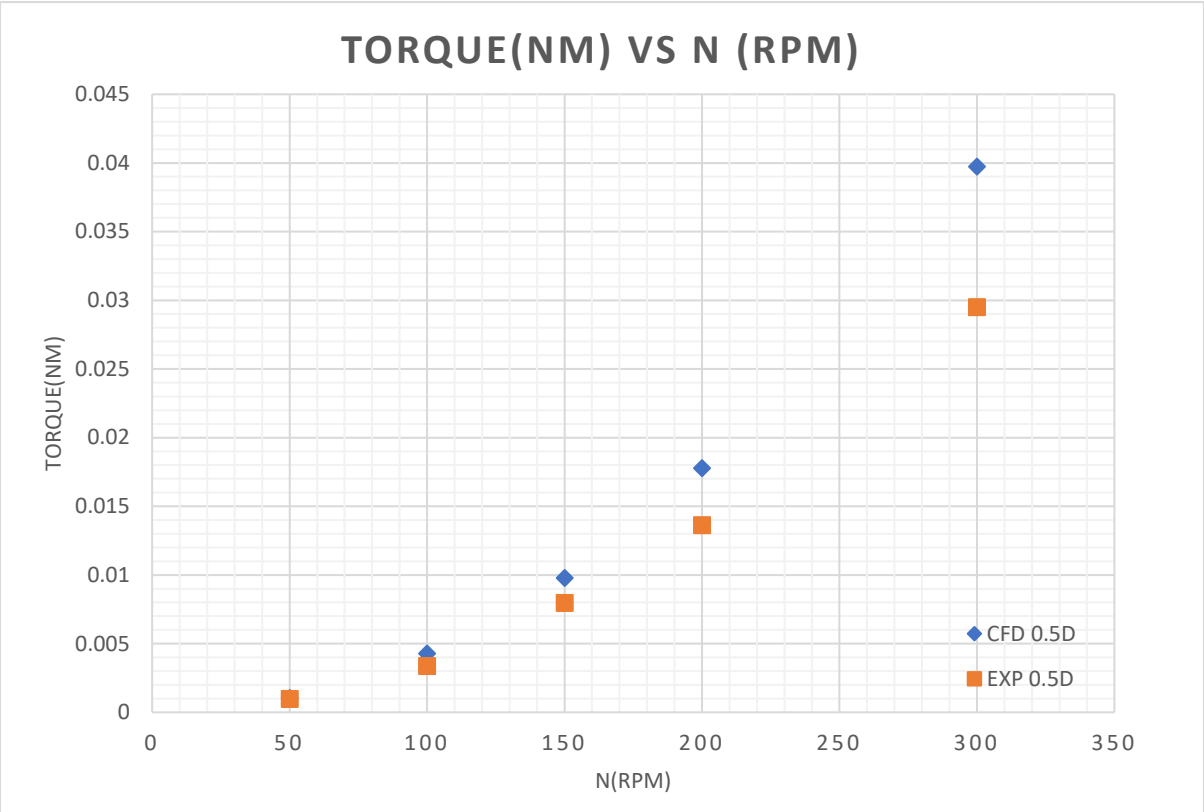

Figure 51 Comparison of torque from experiment and CFD at liquid height 0.5D

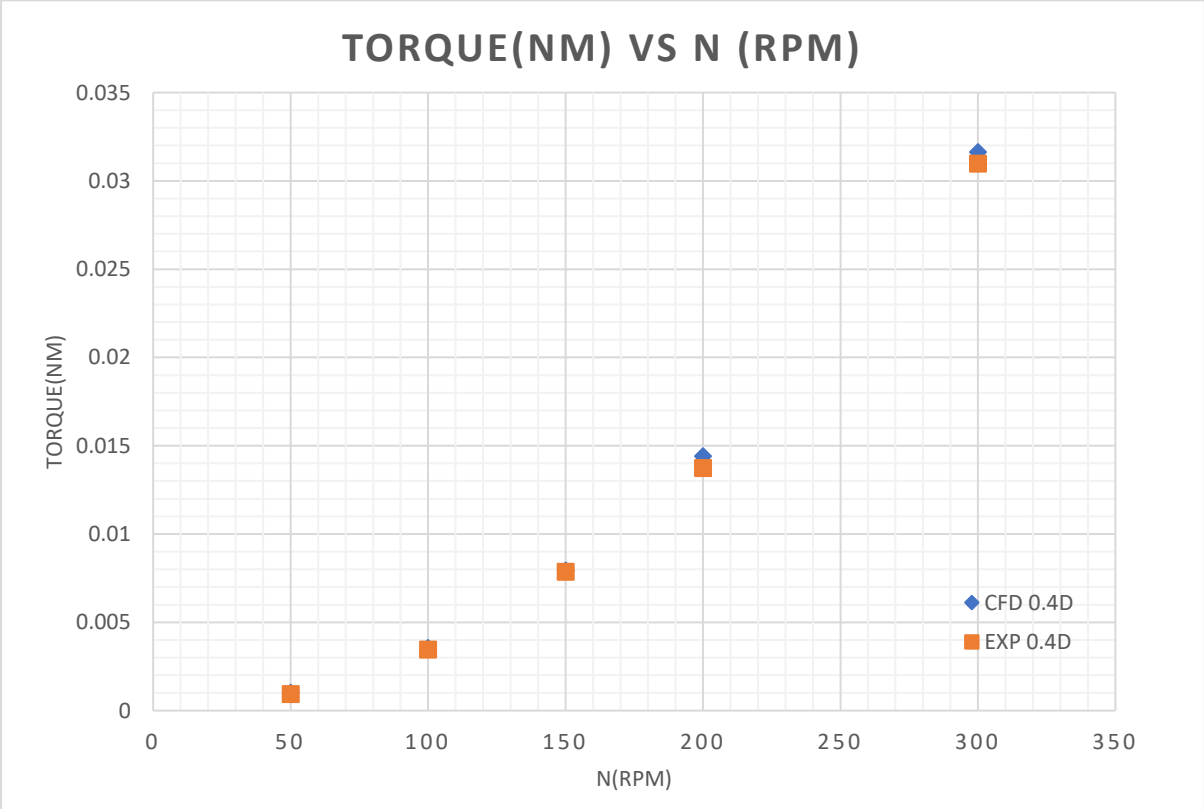

Figure 52 Comparison of torque from experiment and CFD at liquid height 0.4D

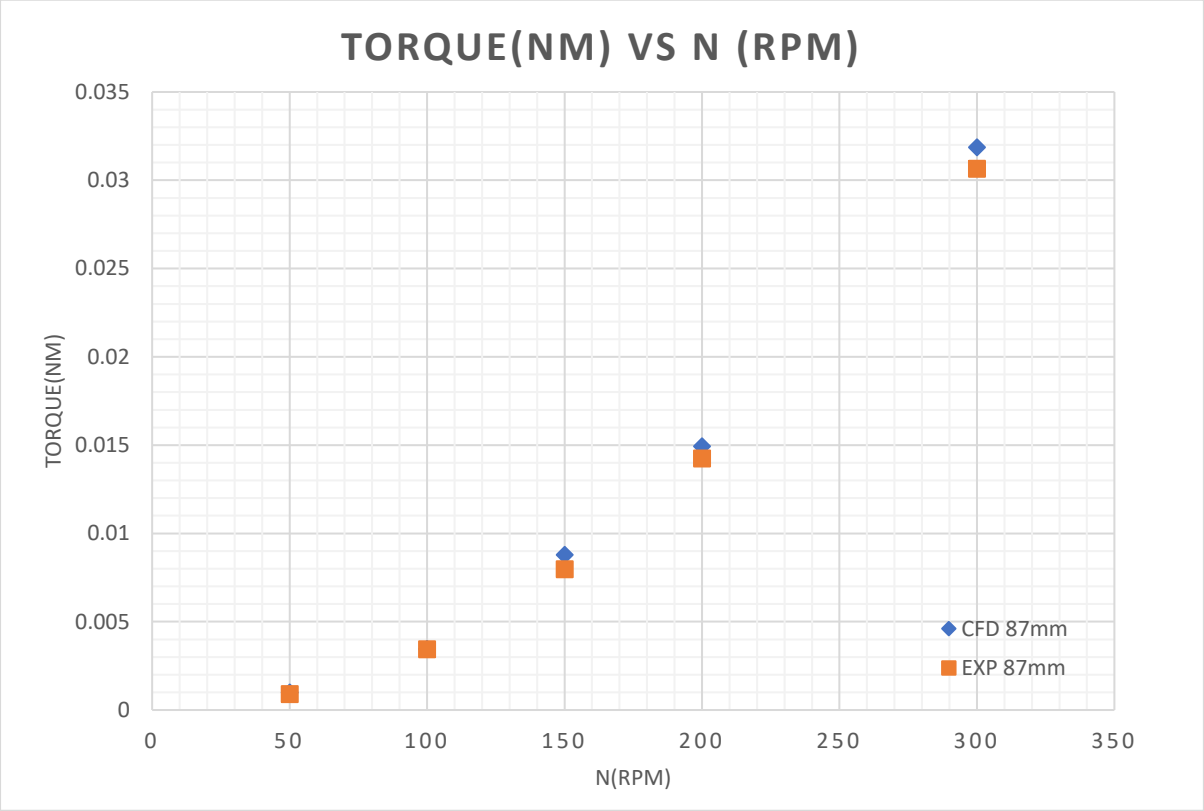

Figure 53 Comparison of torque from experiment and CFD at liquid height 87 mm

The torque computed from the numerical analysis and the experimentally measured torque are in good agreement, as shown in *Figures 48-53.* The discrepancy between the CFD and the result of the experiment is substantially smaller for the liquid height 0.4D and 87 mm, as shown in *Figures 52 & 53. Figures 48,49,50,51,* on the other hand, show that the variance in the result grows as the rotational speed increases. At a liquid height of 0.75D, the difference between the experimental and numerical results is large at higher rotational speed.

4.2 Power consumption

The power consumption is evaluated from the torque according to the *equation.25.*

$$P = \frac{2\pi NM}{60} \tag{25}$$

where N is the impeller revolution (rps), M is the torque (nm) and P is the power (watt).

The power consumption is computed for various liquid heights and revolution speeds, as shown in *Table. 5*

Table 5 Power consumption at various liquid heights

Liquid Heights	N (Rps)	Power consumption for Experiment	Mean value	Power Consumption for CFD	Mean value
H=D	0.833333	0.005869	0.3125	0.005482	0.3695
	1.666667	0.040629		0.045765	
	2.5	0.136744		0.158882	
	3.33333	0.315651		0.381602	
	5	1.063992		1.256245	
0.75D	0.833333	0.005659	0.3188	0.005581	0.3868
	1.666667	0.042173		0.045661	
	2.5	0.136920		0.157376	
	3.33333	0.322191		0.382396	
	5	1.087099		1.343479	
0.6D	0.833333	0.004964	0.2921	0.005455	0.3612
	1.666667	0.035857		0.044111	
	2.5	0.127642		0.150072	
	3.33333	0.298545		0.363582	
	5	0.993812		1.242963	
0.5D	0.833333	0.005137	0.2753	0.005493	0.3647
	1.666667	0.035218		0.044793	
	2.5	0.124851		0.153400	
	3.33333	0.285453		0.372313	
	5	0.926264		1.247578	
0.4D	0.833333	0.004863	0.2848	0.005279	0.2923
	1.666667	0.036204		0.037047	
	2.5	0.123440		0.124629	
	3.33333	0.287349		0.301645	
	5	0.972582		0.992993	
86.88 mm	0.833333	0.004670	0.2851	0.005166	0.2983
	1.666667	0.035890		0.036072	
	2.5	0.124898		0.137686	
	3.33333	0.298065		0.312306	
	5	0.962117		1.000494	

As expected, the CFD and experiment results agree well. When we look at the mean power consumption in *Table 5,* we could see that at the liquid height 0.75D, the power consumption is high in both the numerical analysis and the experiment. However, when it comes to a lower power consumption, the 0.5D liquid height 0.5D in the experiment uses less power. However, the numerical study shows that the 0.4D liquid height consumes the least amount of power. This discrepancy in results could be attributed to measurement inaccuracies during the experiment, because the difference in the mean power usage at liquid heights of 0.4D and 0.5D is 3.4%.

On the other hand, *Table 6* shows that when the impeller uses more power, 0.770H of liquid is above the impeller and 0.229H of liquid is below the impeller. Meanwhile, the numerical analysis shows that the ideal mixing condition is when the liquid is 0.569H above the impeller and 0.430H below the impeller. However, in the experiment, the optimal mixing conditions are when the liquid is 0.655H above the impeller and 0.344H below the impeller.

Table 6 Dimensionless position of impeller

Liquid heights	**Liquid heigh above impeller**	**Liquid height below impeller**
H=D	$0.827H$	$0.173H$
0.75D	$0.770H$	$0.229H$
0.6D	$0.712H$	$0.287H$
0.5D	$0.655H$	$0.344H$
0.4D	$0.569H$	$0.430H$
87 mm	$0.413H$	$0.586H$

According to the literature review[13][14][15], it is noted that the power consumption of the impeller is increased when the liquid level is decreased. However, it is very clear from this study that the power consumption of impeller at various liquid heights are purely depends on the individual impeller. Since both numerical analysis and experimental study clearly predicted that, 0.75D liquid is more power consuming compared to other liquid levels.

4.3 Effect of the impeller rotational speed

This study also looks at the impact of impeller speed on power consumption. According to the literature study [10] the power number is dependent on the third power of the impeller rotational speed in turbulent region flow according to *Equation 4*. Therefore, increasing the rotational speed will increase the power consumption. As shown in *Figures 54 and 55*, the power consumption increases when the rotational speed of the impeller increases. It is clear that both the numerical analysis and the experimental results are accurately predicted.

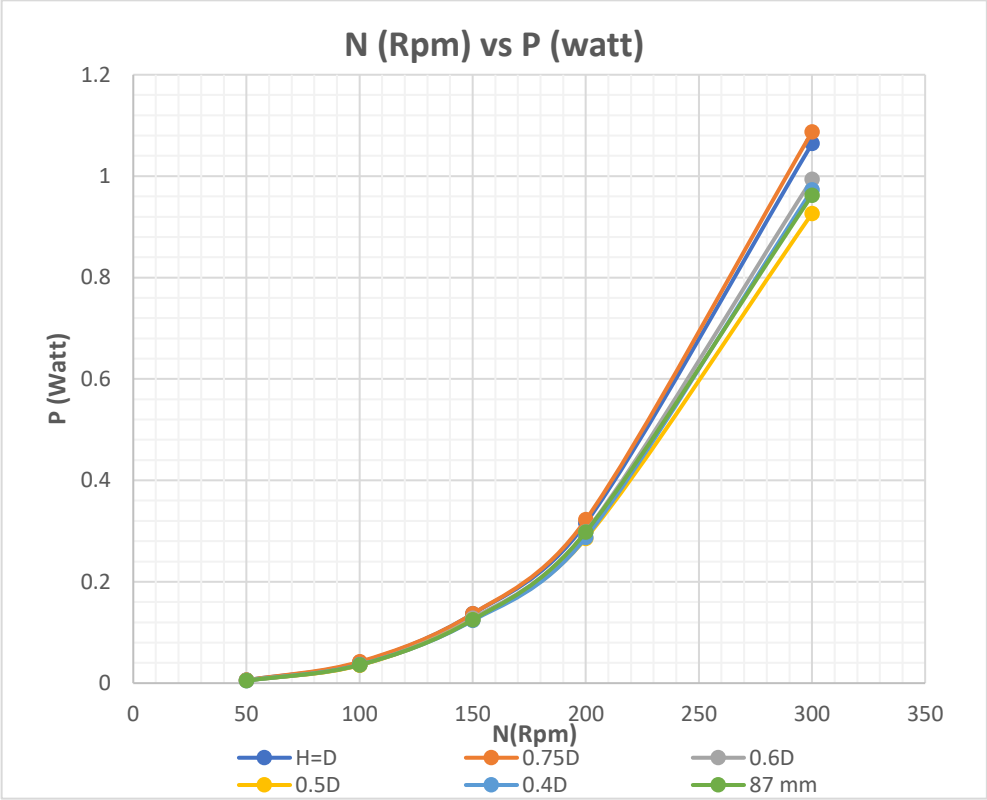

Figure 54 Dependence of power consumption on Rotational speed (Rpm) for experiment

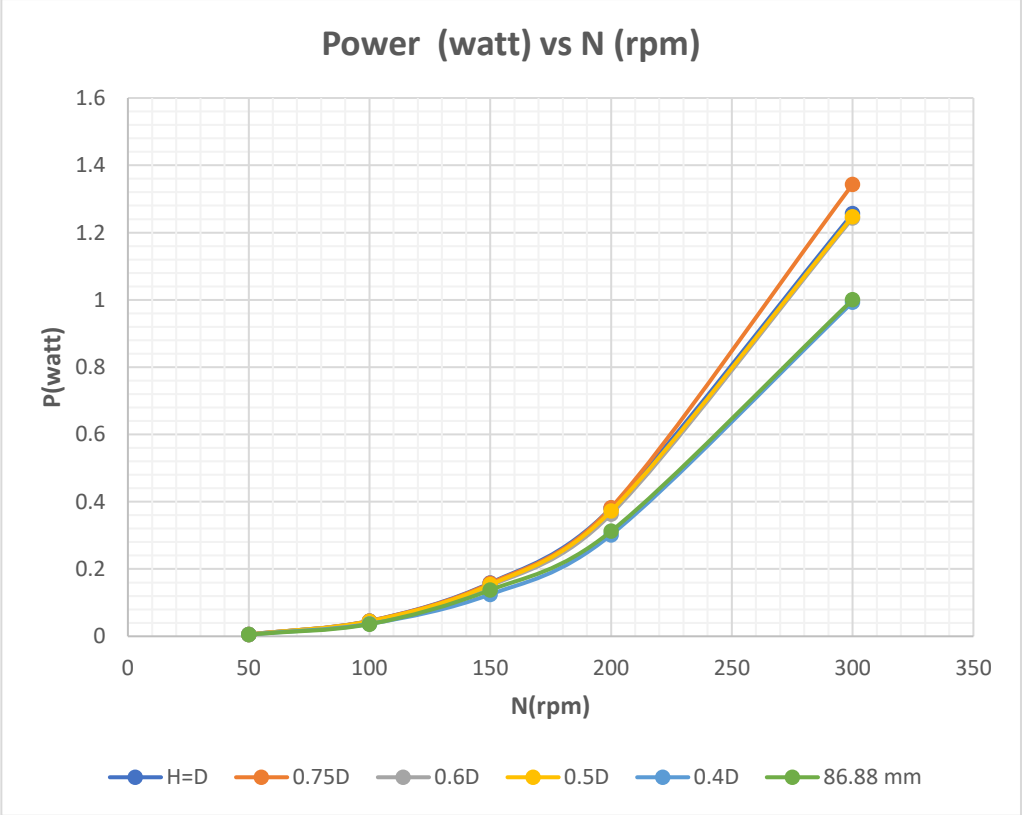

Figure 55 Dependence of power consumption on Rotational speed (Rpm) for numerical analysis

As shown in *Figures 56&57*. The vortex started to form at lower liquid levels as a result of the centrifugal force acting on the rotating fluid. The depth of the vortex increases as the impeller's rotational speed increases. When the impeller hub is exposed to the free surface at a higher rotating speed, the axial fluid flow direction is also shifted to the radial fluid flow direction. This shift was most likely caused by a lack of a sufficiently high layer of liquid above the impeller. *Figure.58* shows changes in liquid circulation.

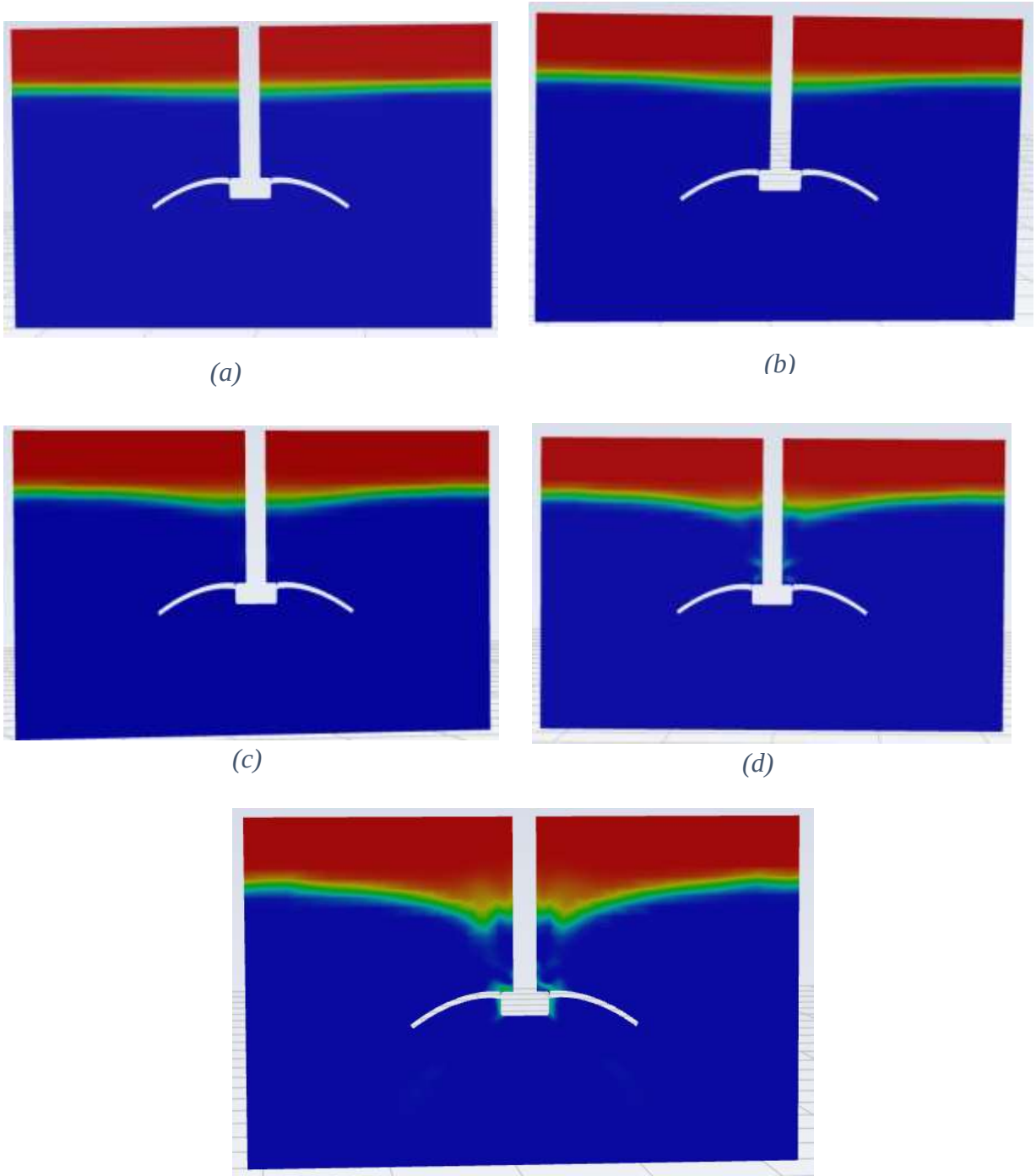

(a) *(b)*

(c) *(d)*

(e)

Figure 56 Contours of volume fraction for various rotational speeds for the liquid height 0.4D : (a) 50 rpm, (b) 100 rpm, (c) 150 rpm, (d) 200 rpm,(e) 300 rpm

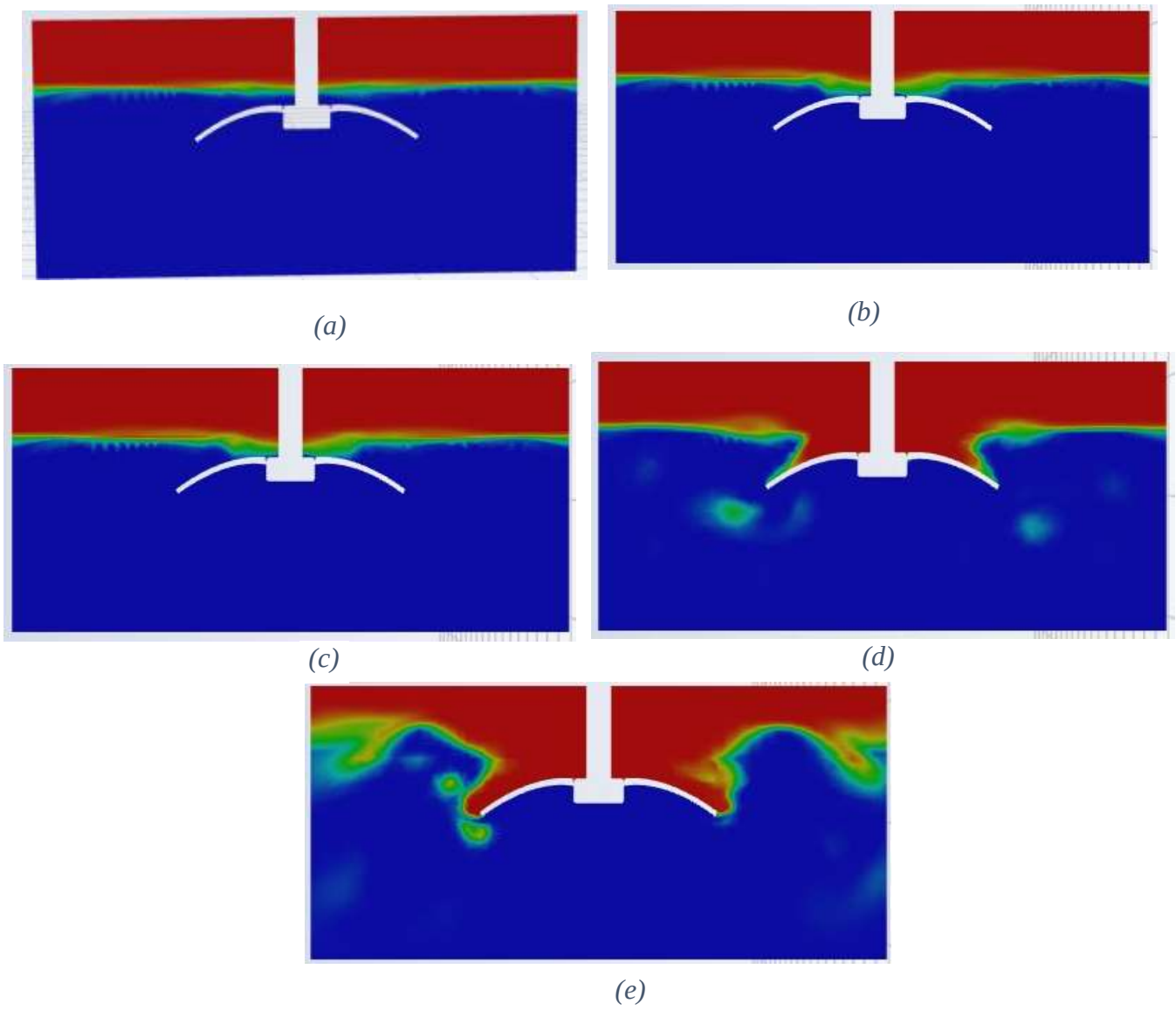

Figure 57 Contours of volume fraction for various rotational speeds for the liquid height 87 mm : (a) 50 rpm, (b) 100 rpm, (c) 150 rpm, (d) 200 rpm,(e) 300 rpm

According to a study in the literature [15] [16],when the impeller hub is exposed to the free surface, the direction of the liquid flow changes from axial to radial circulation, The direction of the liquid flow is also modified from axial to radial circulation, as seen in *Figures 58*. The liquid flow circulation is axial at 150 Rpm, but the liquid flow circulation becomes radial when the impeller rotational speed increases to 200 Rpm and 300 Rpm. This happens because the impeller is exposed to the free surface. The vortex patterns derived from CFD closely resemble the real vortex shapes. A comparison of the vortex at 200 Rpm is shown in *Figure 59.*

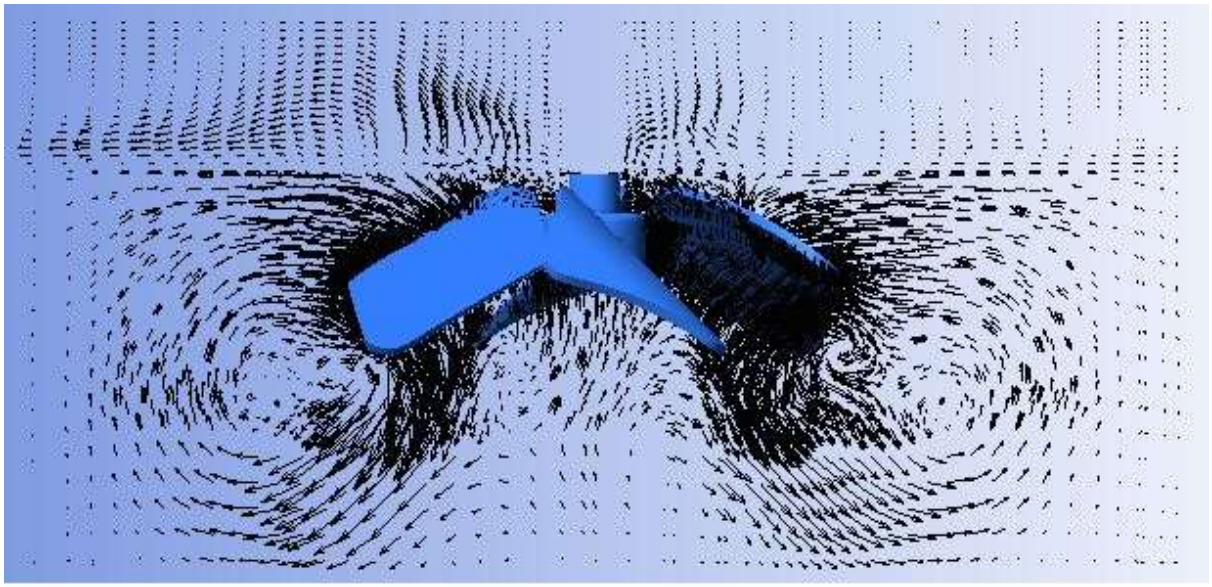

(a)

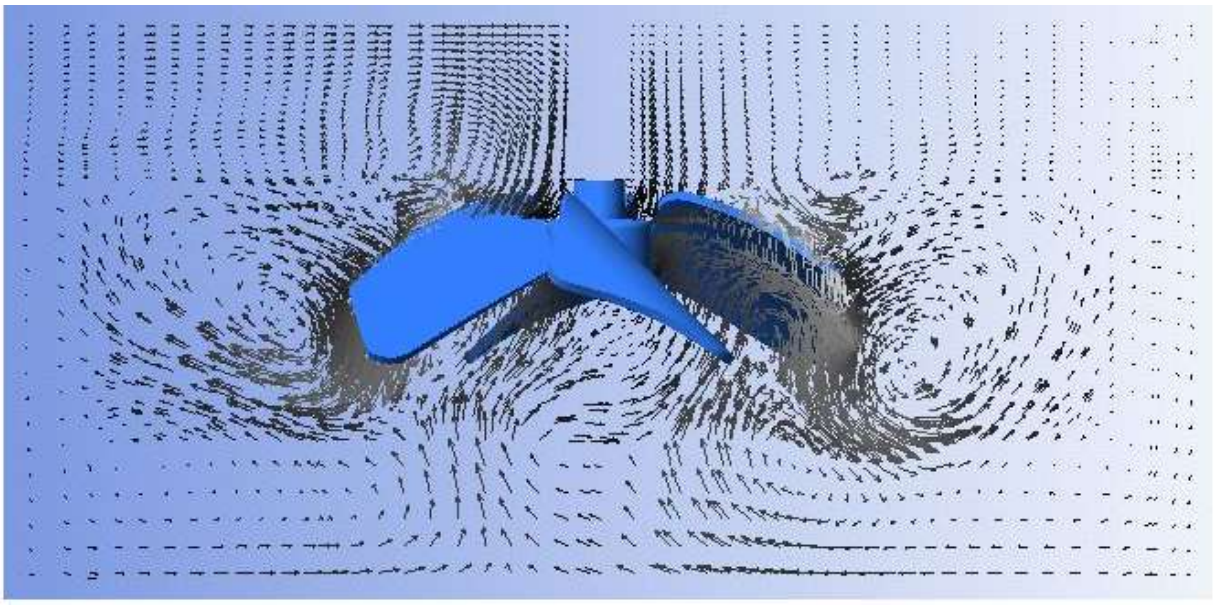

(b)

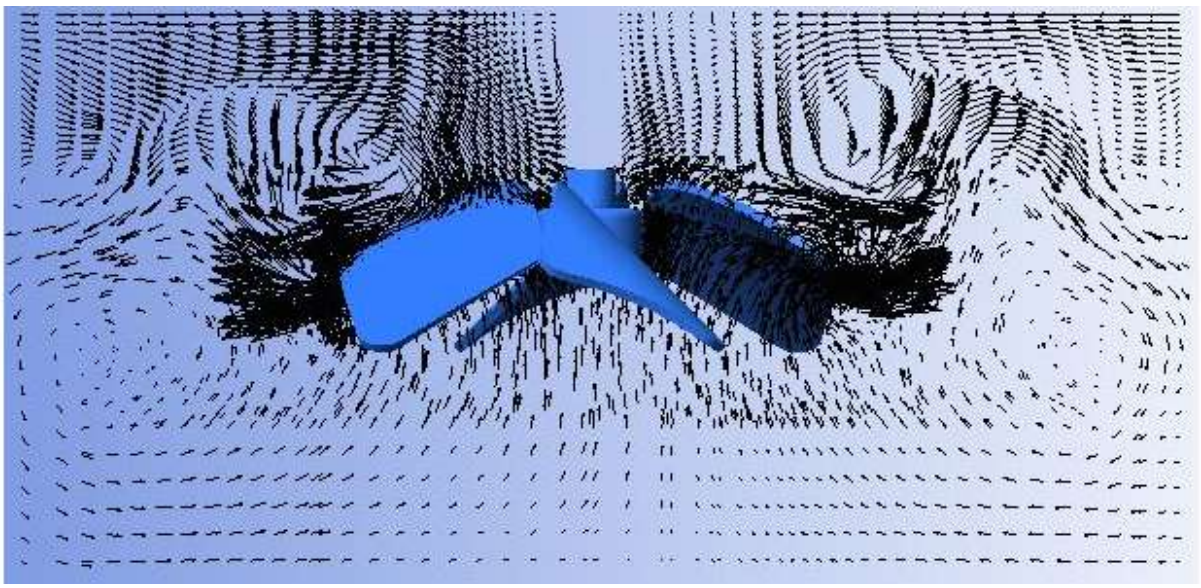

(c)

Figure 58 Change of Fluid flow direction from axial to radial flow direction on liquid height 87 mm at high rotational speed (a) 150 rpm (b) 200 rpm (c) 300 rpm

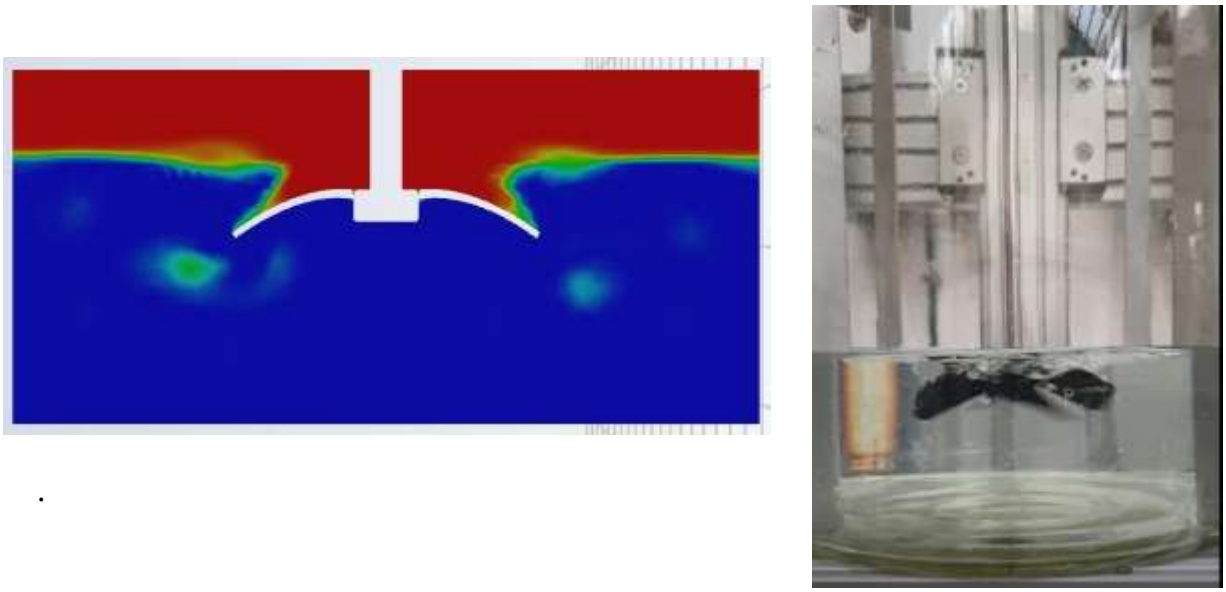

.

Figure 59 The sample comparison of vortex shapes at liquid height 87mm from numerical analysis with experiment at 200 rpm

4.4 Dependence of Power number

The dependence of power number is calculated from the torque on the impeller speed. *Figure 60* depicts the relationship of the power number with Reynolds. According to power number theory, the Reynolds number in the turbulent regime is constant between 30000 and 60000, as expected.

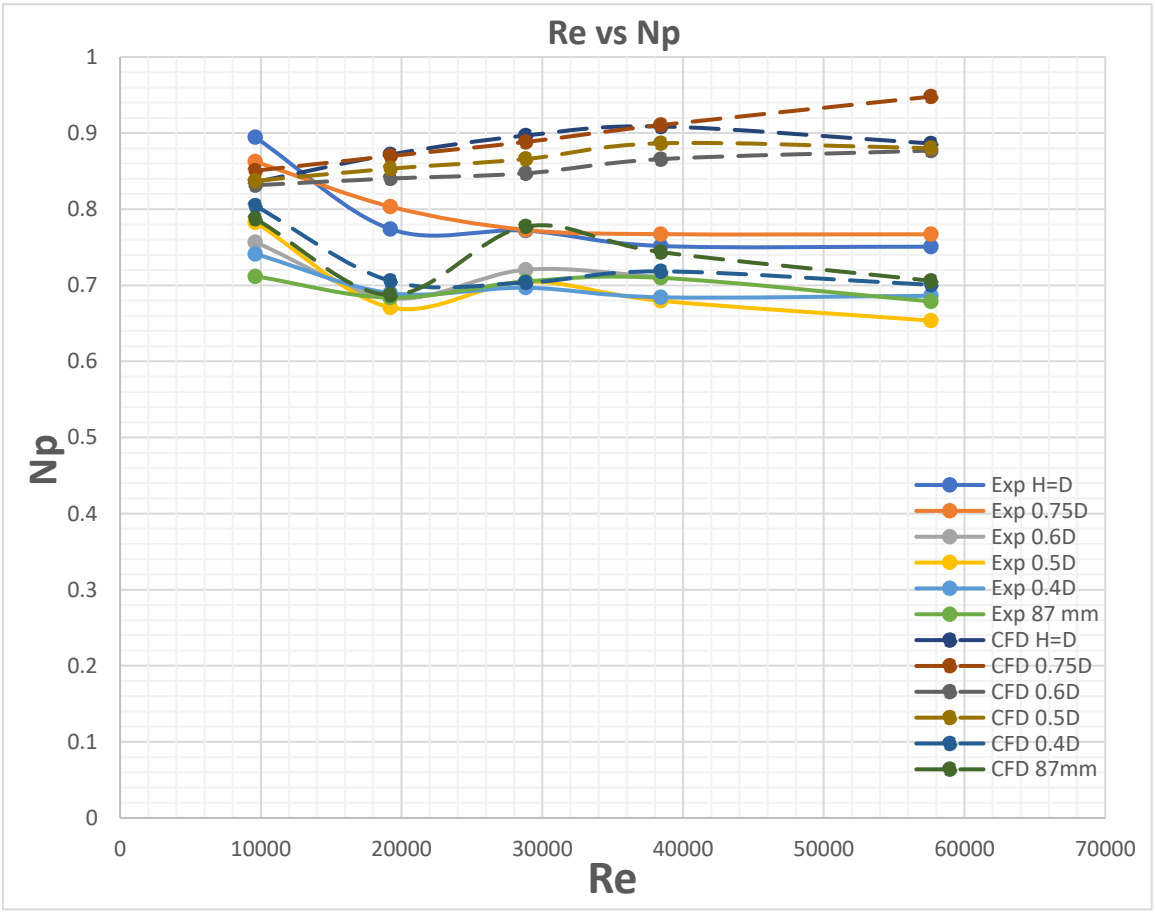

Figure 60 Dependence of power number on Reynolds number

The power numbers calculated for various liquid heights with respective revolution speed using *Equation 4* are shown in *Table 7*

Table 7 Calculated Power number

Liquid Heights	Power number for CFD	Power number for Experiment	Deviation(%)
H=D	0.8355	0.8954	6.5
	0.8718	0.7739	-12.6
	0.8967	0.7718	-16.1
	0.9086	0.7516	-20.8
	0.8863	0.7507	-18
0.75D	0.8505	0.8625	1.3
	0.8698	0.8034	-8.2
	0.8882	0.7728	-14.9
	0.9105	0.7672	-18.6
	0.9478	0.7670	-23.5
0.6D	0.8314	0.7565	-9.9
	0.8403	0.6830	-23
	0.8470	0.7204	-17.5
	0.8657	0.7109	-21.7
	0.8769	0.7011	-25
0.5D	0.8371	0.7829	-6.9
	0.8533	0.6709	-27
	0.8658	0.7047	-22.8
	0.8865	0.6797	-30.4
	0.8802	0.6535	-34.6
0.4D	0.8045	0.7412	-8.5
	0.7057	0.6896	-2.3
	0.7034	0.6967	-0.96
	0.7182	0.6842	-4.97
	0.7006	0.6862	-2
87 mm	0.7874	0.7118	-10.6
	0.6985	0.6837	-2.1
	0.7771	0.7049	-10.2
	0.7436	0.7097	-4.77
	0.7059	0.6788	-3.98

The numerical analysis and experimental findings are in good agreement, as shown in *Table 7*. Although most of the deviations are relatively small, some are significantly larger. The largest deviations are at the 0.5D liquid height for higher rotational speeds.

When we look at the mean value of the power values at different liquid heights, it is considerably easier to understand the power usage. The mean power number is high at liquid height 0.75D in both the CFD and the experiment, as shown in *Figure.61* and *Table 8*. As a result, we conclude that the 0.75D liquid height consumes more energy. There is a disparity between numerical analytical results and empirically measured data when it comes to lower power consumption. *Figure 61* illustrates this point. The mean power number in CFD is lower at 0.4D liquid height, however, the least power number in experiment is at 0.5D liquid height. This may be due to inaccuracies during the measurement because the difference between the mean power number at liquid height 0.4D and 0.5D is just 0.17%.

Table 8 Mean value power number

H/D	Mean power number		Deviation(%)
	CFD	Experiment	
1	0.8798	0.7885	10.3
0.75	0.8934	0.7946	11
0.6	0.8523	0.7144	16.1
0.5	0.8646	0.6983	19.2
0.4	0.7265	0.6996	3.7
0.29	0.7402	0.6978	5.7

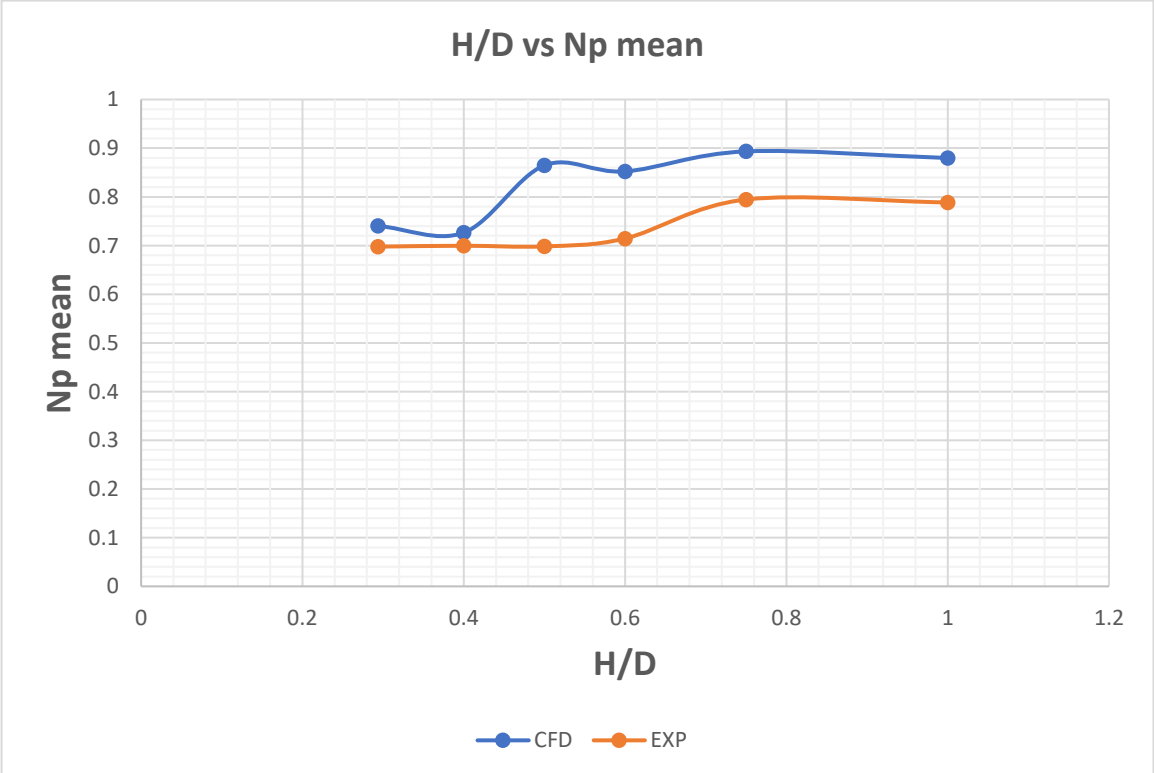

Figure 61 Dependence of power number on liquid height

On the other hand ,when we look at the impact of liquid height above the impeller. *Figure 62* shows that when there is more liquid above the impeller, both the numerical analysis and the experiment show that the power consumption is high. The ideal mixing condition is when there is less liquid above the impeller. As we see from *figure 62*, the liquid heights H = D, 0.75D,0.6D consume more power compared to the lower liquid levels 0.4D,0.5D and 87 mm.

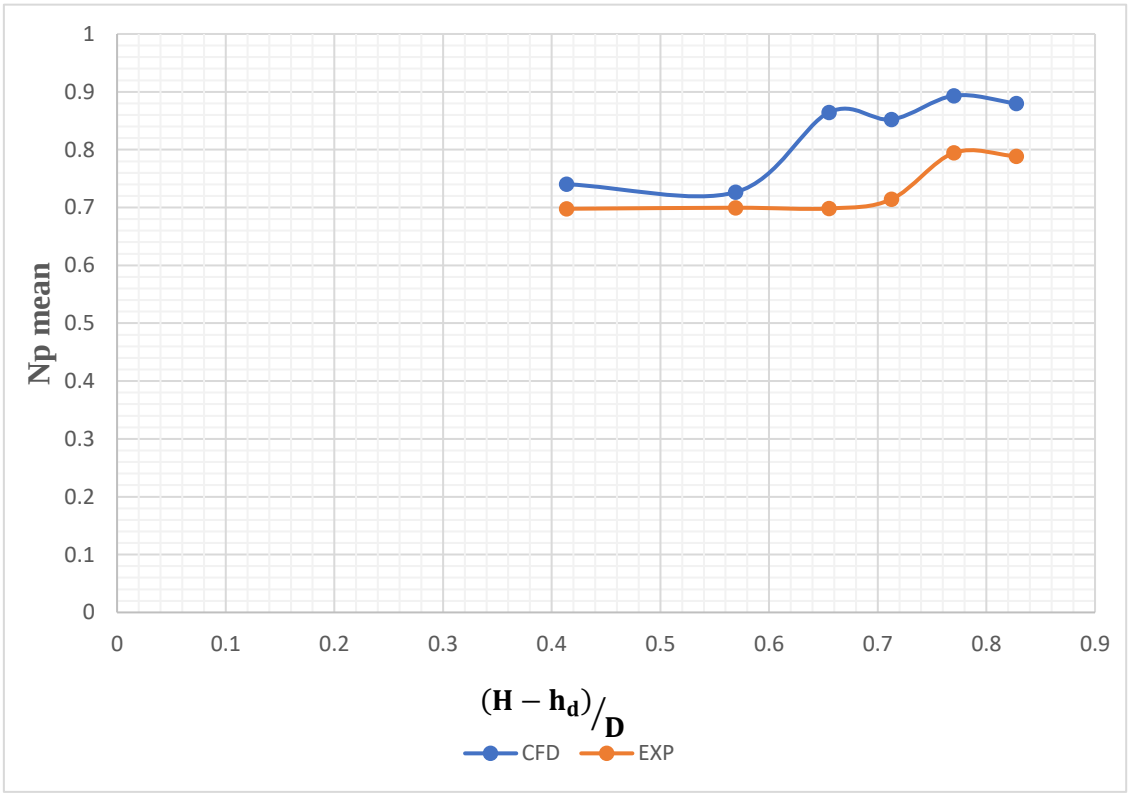

Figure 62 Effect liquid level above the impeller on power consumption

The fraction in the horizontal axis $(H - h_d)/D$ represents the dimensionless liquid level above the impeller from the lowest edge. Where H is the height of the instantaneous liquid height, h_d is the distance of the lower edge of the impeller from the bottom of the tank and D is the inner diameter of the tank.

5. Conclusion and Recommendation

5.1 Conclusion

The major goal of this thesis is to forecast variations in impeller power consumption at non-standard liquid levels. For this, a CFD model is created and the results of the numerical analysis are compared with the experimental data.

To predict the power consumption of impeller, the multiple reference frame approach is used over the sliding mesh approach. Despite the fact that both approaches accurately forecast the power demand, the MRF approach is favoured since it takes less time to compute than the sliding mesh approach. In order to predict the flow near the wall and far from the wall the SST K-omega turbulence model is used. Since it is a combination of the K-omega and K-epsilon. Volume of fluid(VOF) multiphase model is used to analyse because it does not consider each phase independently like the Eulerian-Eulerian multiphase model.

So, the power draws predicted from the numerical analysis are close to the experimental data. Although it accurately predicted the power consumption of the impeller at lower liquid heights of 0.4D and 87 mm, they are slight deviations in the liquid heights of H = D,0.75D,0.6D,0.5 at high rotational speeds, this may be due to inaccuracies during the torque measurement in experiment.

According to the literature review[13][14][15], it is noted that the power consumption of the impeller is increased when the liquid level is decreased. However, it is very clear from this thesis that the power consumption of impeller at various liquid heights are purely dependent on the individual impeller. Since both numerical analysis and experimental study clearly predicted that 0.75D liquid is more power consuming compared to other liquid levels.

On the other hand , according to the study in the literature [14], when the impeller is exposed to the free surface, the axial fluid circulation is transformed into high power consuming radial fluid circulation at higher rotational speed. Thanks to the CFD model, it also predicted the same changes in fluid circulation when the impeller was exposed to the free surface. However, when the liquid level is reduced, the power consumption does not increase, as shown in a study in the literature [14]. As a result, it is evident that the impeller's power consumption at various liquid heights is highly dependent on the individual impeller itself.

Finally, the numerical analysis and experimental results are in good agreement with power number and torque.

5.2 Recommendation

It is clear from this study that the numerical analysis and the experimental results are almost similar. But there was some dissimilarity in results, and to overcome this the mesh has to be finer, especially in the inner fluid domain, to forecast even more precise results. Because the number of cells in the ANSYS 2021 R1 student version is limited. As a result, more precise results from the CFD cannot be predicted. Due to these restrictions, the CFD model is unable to capture air bubbles that occur at lower liquid height. *Figure.63* shows a comparison of air bubbles from the CFD and experiment.

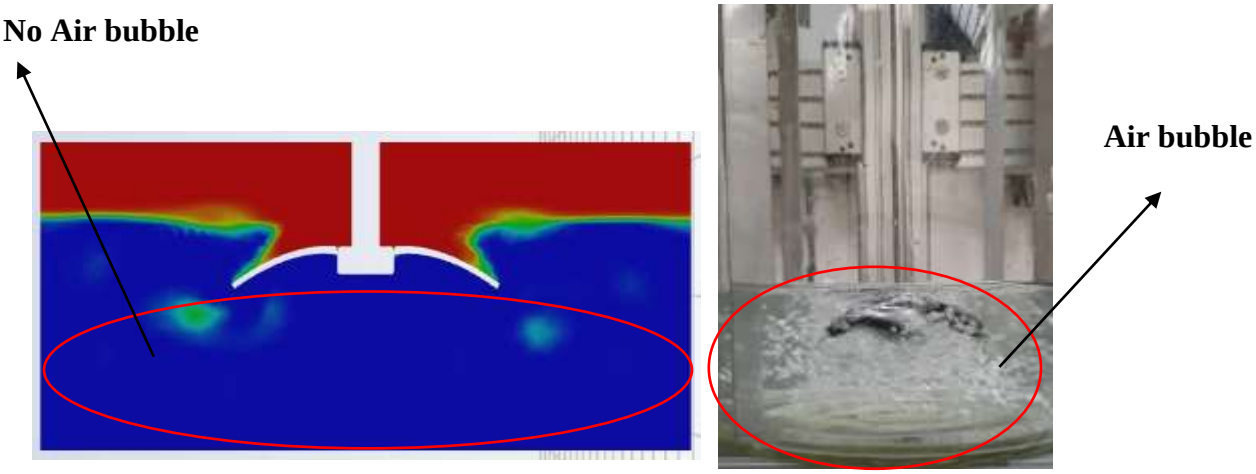

Figure 63 Comparison of air bubble from CFD with experiment at liquid height 87 mm

On the other hand, it is possible that due to the dynamic action of the mixed batch there will be some inaccuracies during torque measurement. So, its need to be avoid in order to get even more accurate results.

Finally, more numerical analysis and experimentation needs to be performed on a greater number of liquid heights with varying rotational speeds are needed for better understanding of the impeller power consumption.

Nomenclature

Variables and parameters

P	Power consumption of impeller (Watt)
N	Impeller Rotation (Rps)
M	Torque (N.m)
Re	Reynolds number (-)
Np	Power number (-)
P	Density (kg/m^3)
D	Diameter of Impeller (m)
L	Impeller spacing (m)
b	Impeller blade height (m)
H	Instantaneous height of the liquid (m)
h_A	Distance of the lower edge of the agitator from the bottom of the tank (m)
μ	Dynamic viscosity (Pa.s)
α_i	Volume fraction (Dimensionless)
ρ_i	Density (kg/m^3)
$\vec{U}$	Velocity Vector (m/s)
τ_i	Stress-strain tensor (N/m^2)
$\vec{g}$	Gravity acceleration (m/s^2)
$\vec{R}_{ij}$	Interaction force between phases (N)
$\vec{F}_i$	Effects of external force, turbulent dispersion force, virtual mass force and lift force(-).
G_k	Generation of turbulent kinetic energy that arises due to mean velocity gradients(m^2/s^3)
K	Turbulence kinetic energy(m^2/s^2)
ω	Specific dissipation rate(1/s)
G_ω	Generation of ω
Y_k Y_ω	Dissipation rate of k and ω due to turbulence

α_k, α_ω Turbulent Prandtl numbers for k and ω respectively (Dimensionless)

S_k , S_ω User defined Source terms

D_ω Cross-diffusion term(m^2/s)

m_{qp} Mass transfer from phase q to phase p ($Kg/m^2\,s$)

m_{pq} Mass transfer from phase p to phase q($Kg/m^2\,s$)

S_{a_q} Source term

$\vec{a}$ Unit vector (Dimensionless)

ω Angular velocity magnitude (rad/s)

$\vec{\omega}$ Rotation vector

$\overrightarrow{u_r}$ Relative velocity (the velocity viewed from the rotating frame) (m/s)

$\vec{u}$ Absolute velocity (the velocity viewed from the stationary frame)(m/s)

$\overrightarrow{u_{wr}}$ Whirl velocity (the velocity due to the moving frame)(m/s)

Acronyms

CFD Computational Fluid Dynamics

VOF Volume of Fluid

PISO Pressure implicit with splitting of operators

SIMPLE Semi-implicit method for pressure-linked equations

SIMPLEC Semi-implicit method for pressure-linked equations consistent

QUICK Quadratic Upstream Interpolation for Convective Kinematics

MRF Multiple reference frame

SST Shear stress transport

BIBLIOGRAPHY

[1] Rushton J H, Costich E W and Everett H J,‘‘ Power characteristics of mixing impellers,” *Chem. Engineering Program*, 46:395-404, 1950; 46:467-79, 1950. (Mixing Equipment Co., Rochester, NY, and Illinois Inst. Technology, Chicago, IL)

[2] Bates R L, P L Foridv and R R Corpstein, “An Examination of Some Geometric Parameters of Impeller Power,” *Ind. Eng. Chem. Process Design Development.* 2,310 ,1963

[3] M.W.Chudacek, ‘‘Solids suspension behaviour in profiled bottom and flat bottom mixing tanks” *M. D. Research Company Pvt. Ltd* ,Volume 40, Issue 3, 1985, Pages 385-392

[4] Su T,Yang F,LiMWu, K, ‘‘Characterization of the hydrodynamics of a covering plate Rushton impeller” *Chin. J. Chem. Eng,*2017, 26, 1392–1400.

[5] Scargiali F, Tamburini A, Caputo G, Micale G, ‘‘On the assessment of power consumption and critical impeller speed in vortexing unbaffled stirred tanks” *Chemical Engineering Research Development*. 2017, 132, 99–110.

[6] Kumaresan T, Jyeshtharaj J.B, ‘‘Effect of impeller design on the flow pattern and mixing in stirred tanks” *Chem. Eng. J.* 2005, 115, 173–193

[7] Ameur H,Kamla Y, Sahel, D. ‘‘Optimization of the Operating and Design Conditions to Reduce the Power Consumption in a Vessel Stirred by a Paddle Impeller”. *Per. Pol. Mech. Eng.* 2018, 62, 312–319

[8] Haruki Furukawa,Toshiki Kamiya, and Yoshihito Kato ‘’Correlation of Power Consumption of Double Impeller Based on Impeller Spacing in Laminar Region’’ 466-8555,2019

[9] Tao yang and Koji takashi, ‘‘Effect of Impeller Blade Angle on Power Consumption and Flow Pattern in Horizontal Stirred Vessel” *Journal of Chemical Engineering of Japan,* Vol. 43, No. 8, pp. 635–640, 2010

[10] Chang and Gwo-Ming, "Power consumption in single-phase agitated vessels provided with multiple impellers" (1993). Theses. 1727.

[11] M E Matlakala, ‘‘Influence of Impeller Diameter on the Performance of Centrifugal pumps”. *IOP Conf. Ser.: Mater. Sci. Eng.* 655 012009,2019.

[12] Joannis Markopoulos, Evanthia Babalona, and Evanthia Tsiliopoulou, ‘‘Power Consumption in Agitated Vessels with Dual Rushton Turbines: Baffle Length and Impeller Spacing Effects” *Chemical Engineering Technology*. 2004, 27, No. 11

[13] C Devarajulu, M. Loganathan, ‘‘Effect of Impeller Clearance and Liquid Level on Critical Impeller Speed in an Agitated Vessel using Different Axial and Radial Impellers”, *Journal of Applied Fluid Mechanics*, 2016.

[14] Nobuhiro Yasui, Haruki Furukawa, Ryo Nagumo, ‘‘Effect of Liquid Height on Power Consumption of Two-Blade Wide Paddle Impeller”, November 2016, *KAGAKU KOGAKU RONBUNSHU* 42(6):187-191.

[15] Stelmach, Kuncewicz, Rieger, Moravec, Jirout, “Increase in mixing power when emptying tanks with turbine-blade mixers”, *Chemical Industry* , Vol. 99, no. 2, 2020

[16] Rieger, Jirout, Moravec, Stelmach, Kuncewicz, ‘‘The phenomenon of an increase in the demand for mixing power during emptying the tank”, *Chemical industry 9*8 (6), 2019

[17] Paulv E L, Atiemo-Obeng V A & Kresta S. M. (2004),‘‘Handbook of industrial mixing: Science and practice Wiley-Interscience

[18] Wadnerkar D, R P Utikar, M. O. Tade, and V. K. Pareek, “CFD Simulation of Solid Liquid Stirred Tanks.” *Advanced Power Technology* 23: 4,2012

[19] Wadnerkar D,M. O. Tade, V. K. Pareek, and R. P. Utikar. “CFD Simulation of Solid–Liquid Stirred Tanks for Low to Dense Solid Loading Systems.” *Particuology* 29: 16–33. 2016

[20 Ljungqvist M, and A. Rasmuson, “Numerical Simulation of the Two-Phase Flow in an Axially Stirred Vessel.” *Chemical Engineering Research and Design* 79: 533–46,2001

[21]‘‘Fluid flow direction in mixing”, http://www.visserssales.com/Blog/Difference-Between-Axial-Flow-Impellers-and-Radial-Flow-Impellers.w

[22]‘‘Types of axial flow impeller” https://dynamixinc.com/mixing-101-the-basic-principles-of-mixing-and-impellers/

[23] Ramesh K. Goel, Joseph R.V. Flora, and J. Paul Chen ,‘‘Flow Equalization and Neutralization” 2007

[24] Divya Rajavathsavai, Akhilesh Khapre and Basudeb Munshi,‘‘ Study of mixing behavior of CSTR using CFD” *Brazilian Journal of Chemical Engineering* 31(1):119 – 129, 2014

[25] Ansys, “ANSYS FLUENT 12.0 Theory Guide - ‘‘Equations for a Rotating Reference Frame” https://www.afs.enea.it/project/neptunius/docs/fluent/html/th/node30.htm

[26] Ansys, “ ANSYS FLUENT 12.0 Theory guide – “ Force moment” https://www.afs.enea.it/project/neptunius/docs/fluent/html/th/node414.htm#sec-report-

[27] Moodle “CFD Application in process engineering’’ – “ Mesh process in ANSYS meshing” https://moodle-vyuka.cvut.cz/pluginfile.php/60536/mod_resource/content/1/Mesh-Intro_15.0_L03_Introduction_to_Ansys_Meshing.pdf